
Article:
Lewis, C.J., Sancho, C., McDonald, E.V. et al. (5 more authors) (2017) Post-tectonic landscape evolution in NE Iberia using staircase terraces: Combined effects of uplift and climate. Geomorphology, 292. pp. 85-103. ISSN 0169-555X

https://doi.org/10.1016/j.geomorph.2017.04.037

Post-tectonic landscape evolution in NE Iberia using staircase terraces: combined effects of uplift and climate

Claudia J. Lewis[1], Carlos Sancho[2*], Eric V. McDonald[3], José Luis Peña-Monné[4], Emilio L. Pueyo[5,6], Edward Rhodes[7], Mikel Calle[8], Ruth Soto[5,6]

[1] Earth and Environmental Sciences Division, Los Alamos National Laboratory, 87545 Los Alamos, NM, USA

[2] Ciencias de la Tierra, Universidad de Zaragoza, Pedro Cerbuna 12, 50009 Zaragoza, Spain

[3] Desert Research Institute, 2215 Raggio Parkway, Reno, NV, USA

[4] Geografía y Ordenación del Territorio, Universidad de Zaragoza, Pedro Cerbuna 12, 50009 Zaragoza, Spain

[5] Instituto Geológico y Minero de España, Unidad de Zaragoza, Manuel Lasala 44, 50006 Zaragoza, Spain

[6] Unidad Asociada en Ciencias de la Tierra IGME-Universidad de Zaragoza

[7] Department of Geography, The University of Sheffield, Sheffield S10 2TN, UK

[8] Museo Nacional de Ciencias Naturales, CSIC, José Gutiérrez Abascal 2, 28006 Madrid, Spain

*** Corresponding author:**

Carlos Sancho Marcén

Departamento de Ciencias de la Tierra

Universidad de Zaragoza

Pedro Cerbuna, 12

50009 Zaragoza

Spain

Email: csancho@unizar.es

Phone: +34976761091

Abstract

River incision into bedrock resulting from the combined effects of tectonic uplift and climate governs long-term regional landscape evolution. We determined spatial and temporal patterns of post-orogenic stream incision from a sequence of well-preserved staircase terraces developed over the last 1 Ma in the Central Pyrenees and its southern foreland Ebro basin (NE Spain). Extensive remnants of ten vertically separated terraces (Qt1 to Qt10, from oldest to youngest) were mapped along 170 km of the Cinca River valley, transverse to the Pyrenean mountain belt. Multiple outcrops appear in the upper reach of the valley (Ainsa sector, 50 km from headwaters) as well as in the lower reach (Albalate sector, 125 km from headwaters). Fluvial incision into bedrock was calculated using (i) differentially corrected GPS measurements of the altitude of straths and (ii) numerical dating of alluvial sediments from the lower terraces (Qt5 to Qt9) by Optically Stimulated Luminescence, previously reported by Lewis et al. (2009), and supplemented with new dates for the upper terraces (Qt1, Qt2 and Qt3) based on palaeomagnetism and supported by soil development. Considering altitude differences and the elapsed time between successive well preserved terrace couples (Qt3-Qt7, Qt7-Qt9 and Qt9-Active channel), mean bedrock incision rates ranged from 0.76 to 0.38 m ka^{-1}, at the upper reach of the valley (Ainsa section), and from 0.61 to 0.20 m ka^{-1}, at the lower reach (Albalate section). River incision along the valley produced vertically separated, near-parallel longitudinal terrace profiles evidencing a rapid near-uniform regional uplift as response to (i) the tectonic lithospheric thickening in NE Iberia and (ii) the erosional download rebound related to the Ebro basin exorheism. Moreover, a subtle upstream divergence of strath profiles

may have been a consequence of an increase in uplift rate toward the head of the valley. Additionally, incision rates changed over time as indicate results from the lower reach (Albalate section); the maximum rate was 1.48 m ka^{-1} between Qt7 (61 ka) and Qt8 (47 ka), and the minimum rate was 0.11 m ka^{-1} between Qt3 (401 ka) and Qt5 (178 ka). The highest incision rates were produced after the Marine Isotope Stage 4 most likely in response to (i) an increased snowmelt discharge during the subsequent deglaciation related to the last maximum advance of glaciers in the southern Pyrenees, and (ii) a limited width of the valley after Qt7 formation, resulting from the deactivation of the westward river migration. Therefore, incision rates over the last 1 Ma in the Cinca River valley were basically controlled by near-uniform bedrock uplift, in the context of climate variability. The results reported in this study represent significant data on fluvial incision in NE Iberia, and provide an assessment of the regional post-tectonic landscape evolution.

Key words: Fluvial incision, Staircase terraces, Uplift, Climate change, Mid- to Late Pleistocene, Southern Pyrenees and Ebro Basin

1. Introduction

Landscape evolution represents a morphotopographic balance resulting from interactive competition between tectonics, climate and denudation processes (e.g., Burbank and Anderson, 2001; Willet et al., 2006; Cloetingh and Willett, 2013). Fluvial terraces are excellent geomorphic markers that have been used extensively to document landscape evolution (e.g., Bridgland and Westaway, 2008; Westaway et al., 2009). Long-term geomorphic configuration of fluvial systems involves the entrenchment of river valleys and the creation of staircase terrace sequences in response to the basic driving forces of regional climate, tectonic uplift and base level (e.g., Bridgland, 2000; Starkel, 2003; Gibbard and Lewin, 2009; Westaway et al., 2009; Stokes et al., 2012; Pazzaglia, 2013; Wang et al., 2015).

Terraces as geomorphic markers to assess fluvial incision and landscape development have been commonly used worldwide under different orogenic and post-orogenic geodynamic contexts. At a regional scale, deciphering the nature and history of fluvial incision in the Iberian Peninsula, which has an extensive network of terraces, has been limited and remains an unsolved challenge. Undoubtedly, the general lack of well chronologically referenced terrace systems (Santisteban and Schulte, 2007) is determinant. Several regional studies on river incision have been reported by Cunha et al. (2005, 2008, 2012) and Martins et al. (2009, 2010) in the Portuguese reach of the Tagus River, Antón et al. (2012) and Silva et al. (2013, 2016) in the Spanish reaches of the Duero and Tagus rivers, Stange et al. (2013; 2016) in the Segre River valley in the southern Pyrenees, Soria-Jáuregui et al. (2016) in the upper sector of the Ebro River valley, Scotti et al. (2014) and Giacheta et al. (2015) in the Iberian Ranges (NE Spain),

and Viveen et al. (2014) in the Miño River basin from northwest Iberian. Additionally, data on regional fluvial incision need to be integrated within the geodynamic models explaining the Iberian topography and with the regional Pleistocene climate reconstruction for southwestern Europe.

The Spanish Pyrenees and the adjacent Ebro foreland basin comprise an outstanding area to deduce post-orogenic river incision rates and landscape development from staircase terraces and to discuss the uplift mechanisms and the climate changes involved. In this paper we use a well characterized sequence of staircase terraces located along the Cinca River valley, one of the most important Pyrenean tributaries of the Ebro River in northeast Iberia, to evaluate post-tectonic landscape evolution. Reported results are based in a combination of (i) reconstructed longitudinal strath profiles starting from previously mapped terraces (Sancho, 1988), (ii) numerical ages using optically stimulated luminescence (OSL) and supported by time-related trends in soil development (Lewis et al., 2009), and (iii) new palaeomagnetic and soil stratigraphic data. We use our results to deduce spatial and temporal patterns in river incision rates and to discuss the combined action of uplifting and climate change governing the formation of staircase terrace sequences in NE Iberia.

2. Study area

2.1 The Cinca River valley

The Cinca River valley straddles the south-central Pyrenees and the northern Ebro basin (NE Spain) (Figs. 1, 2A). Mean annual precipitation varies from > 2,000 mm in the high Pyrenees to < 400 mm in the semiarid Ebro basin. The Cinca River is 170 km long;

it has a drainage area of 9,700 km^2 and a mean annual flood discharge of 79 m^3/s. The natural fluvial regime of the Cinca River is altered by the presence of two large reservoirs: the El Grado and Mediano dams (Fig. 3A).

The headwaters area of the Cinca River is glaciated and is located in the Pyrenean Internal Sierras (Monte Perdido summit: 3,355 m a.s.l.). The Cinca River drains to the south and is perpendicular to the Pyrenean belt, joining the larger and eastward-flowing Ebro River in the Ribarroja reservoir (90 m a.s.l.) in the central Ebro Basin. This river confluence is more than 100 km up gradient from the Mediterraean Sea (Fig. 1). The Cinca River in the upper valley (from headwaters to Ainsa; Figs. 1, 3A) is a mixed bedrock-alluvial channel, whereas the Cinca River in the lower valley (from Basbastro to the mouth into the Ebro River; Figs. 1, 3A) is an alluvial gravel channel. Several slight knickpoints can be identified along the active channel profile: however, only the knickpoint located at El Grado (External Pyrenees) is noticeable (Figs. 2B, 3A).

2.2 Geologic setting

Geologically, the Cinca River valley is excavated in the Pyrenean belt and the adjacent Ebro foreland basin (Fig. 2A). The Pyrenees constitutes a WNW-ESE striking, narrow asymmetric alpine chain with a mainly southward vergence, developed from the Late Cretaceous to the Early Miocene. This structural setting was formed in response to the partial subduction of the Iberian lithosphere underneath Europe (e.g., Muñoz, 2002). The southern central Pyrenees comprise part of the Axial Zone, formed by a basement and a series of imbricated thrust sheets, involving Mesozoic to Eocene cover rocks and affecting synorogenic Tertiary materials (e.g., Martínez-Peña and Casas-Sainz, 2003).

Specifically, the Cinca River valley is located at the western border of the South Pyrenean Central Unit that is characterized by north-south oblique structures that control the north-south alignment of the Cinca River (Martínez-Peña et al., 1995). From a stratigraphic point of view, the Cinca River traverses the western sector of the Graus-Tremp basin (the Ainsa sub-basin) (Fig. 2B), a piggy-back basin filled with Palaeocene-Eocene deposits (Puigdefábregas and Souquet, 1986).

The Tertiary Ebro basin was formed during the Palaeogene as a consequence of flexural subsidence related to growth of the surrounding mountain chains, particularly the Pyrenees. Sedimentation into the closed basin continued under conditions of continental internal drainage during Oligocene and Miocene times (Muñoz et al., 2002; Costa et al., 2010) (Fig. 2B). This sedimentary regime persisted until the end of the late Miocene (between 12.5 and 8.5 Ma) when the internal drainage of the Ebro basin ended due to aggradation of the lacustrine system and extensional geodynamic conditions in the western Mediterranean basin (Garcia-Castellanos et al., 2003). The Ebro basin was subsequently opened when headward erosion of coastal drainage captured the internally draining system. The Ebro sedimentary basin was then incised and previous depositional units were excavated and transported to the coastal Mediterranean.

Erosional activity of the drainage in the Pyrenees and the Ebro Basin persisted throughout the Quaternary. Subsequent fluvial activity developed extensive staircase terrace sequences along the Ebro drainage system (e.g., Gutiérrez and Peña, 1994; Peña, 1994). The earliest evidence of alluviation in the exoreic Ebro basin is at ca. 1.28

Ma in the Alcanadre River valley, a tributary of the Cinca River (Duval et al. 2015; Sancho et al., 2016).

2.3 Approach to the Cinca River terrace sequence

Two basic configurations of stream terraces, strath and fill terraces, are commonly differentiated, based on the morphology of the erosional surface and thickness of alluvial sediments (Bull, 1991; Pazzaglia, 2013). A strath terrace is characterized by a subhorizontal erosional surface carved into bedrock mantled with a thin mobile alluvial cover of a bedrock channel that does not exceed the depth of scour of the stream. In contrast, fill terraces are characterized by an irregular basal surface covered by a layer of thick alluvium that accumulates when the channel vertically exceeds the depth of scour, during periods of valley aggradation (Wegmann and Pazzaglia, 2009; Pazzaglia, 2013). The thickness of the alluvial cover is a long-discussed criterion to distinguish between both types of terrace (Pazzaglia, 2013). Mobile alluvial cover associated with strath terraces rarely exceeds 5 m in thickness even for large watersheds, while greater alluvial thickness is usually related to fill terraces (Pazzaglia, 2013).

The studied terrace sequence in the Cinca River valley consists of 10 extensive paired cyclic stream terraces (Sancho, 1988; Lewis et al., 2009). The mean thickness of the alluvial mantle covering the straths is around 5 m, ranging from 8 m for the oldest terraces to 3 m for the youngest terraces. The general morphology of strath surfaces is broadly subhorizontal. Given this description, the Cinca River terrace sequence is closer to a strath relative to a fill terrace and displays a strath-like terrace. We

recognize that in places, a near-fill terrace configuration related to slight valley aggradations could be considered.

3. Methods: using terrace straths to measure river incision

Determination of the river incision rate (e.g., Burbank and Anderson, 2001) for a point along a river valley is given by the ratio between the height (m) of the terrace strath above the active channel and the timing (ka) of terrace formation. We expanded this approach to calculate the river incision rate between a given pair of terraces; the fluvial incision rate ($I_{Qti-Qtj}$) (m/ka) between any two terraces Qti and Qtj, is given by the relation:

$$I_{Qti-Qtj}=H_{Qti-Qtj}/T_{Qti-Qtj}$$

where $H_{Qti-Qtj}$ is the difference of altitude (m) of the terrace straths Qti and Qtj, and $T_{Qti-Qtj}$ is the elapsed time (ka) between them.

We use the terrace straths rather than the terrace treads to measure river incision rates (Wegmann and Pazzaglia, 2009) because tread surfaces can be subsequently modified through both aggradation or degradation. Observations of terrace stratigraphy indicate that in places the terrace surface has been aggraded through deposition of lateral alluvial and aeolian sediments or degraded through erosion removal and lowering of the original terrace surface as indicated by severely truncated or missing soil profiles.

3.1 Height of terrace straths and the active channel

Collecting and assessing height measurements of bedrock strath surfaces requires compiling a detailed regional geomorphological framework. Geomorphic mapping was undertaken on an aerial photographic base (1:18,000 in scale) and was extensively field checked along the Cinca River valley. Ten terraces were firstly identified (Qt1 to Qt10, from higher to lower) from their altitudinal position (Sancho, 1988; Lewis et al., 2009). Correlation of terraces was primarily based on geomorphologic and stratigraphic relationships between terraces and was reinforced with soil development and numerical dating. Elevations of the differentiated strath terrace surfaces and the Cinca active channel were measured to sub-meter accuracy using a global positioning system (GPS) differentially corrected to a permanent base station. Measurements were occasionally supplemented by data from 1:25,000-scale topographic maps. Height measurements allowed reconstruction of accurate profiles of strath terraces and the active channel.

3.2 Chronology of terraces

Timing of strath preservation is broadly based on the basal age of overlying fluvial deposits. We used numerical dates previously provided by Lewis et al. (2009), based on OSL of quartz grains dating and supported by soil stratigraphy. These data are available only for the lower terraces (from Qt5 to Qt9) corresponding to both the Penultimate and the Last Glacial cycles. In this study we provide new chronological evidence for the older terraces using paleomagnetic analysis and time-related trends in soil development.

3.2.1 Paleomagnetic sampling and laboratory procedures

Characterization of the paleomagnetic polarity has been a powerful tool for unravelling terrace ages since the pioneering work of Pevzner (1970). Subsequent applications have focused on locating the Brunhes/Matuyama (B/M) boundary (Dubar and Semah, 1986; Jacobson et al., 1988) or even shorter polarity events within the Brunhes and Matuyama periods (Li et al., 1997). Paleomagnetic analysis was conducted on the Cinca River alluvium overlying the strath terraces to identify the location of the B/M boundary. Previous results in the Central Ebro Basin (Gil et al., 2013) and in the Alcanadre River (tributary of the Cinca River; Calle et al., 2015; Sancho et al., 2016) allowed us to be confident of the suitability of the method provided that an adequate sampling was guaranteed (Gil Garbi, 2017).

Sampling for paleomagnetic analysis was performed in 13 pits excavated in the upper terraces along the valley (from Qt1 to Qt7). Siltstone layers within alluvial sequences were the main targets to ensure a stable paleomagnetic signal. Sampling tools designed for unconsolidated sediments were used instead standard drilling machines. Subsequent consolidating techniques using non-magnetic chemical compounds (sodium silicate and alumina cement) were used to obtain standard and stable paleomagnetic specimens (Pueyo et al., 2006). Oriented blocks were occasionally sampled.

Present-day declination (~ 1° 30'W) during the sampling was corrected in the core orientations (NOAA's National Geophysical Data Center, https://www.ngdc.noaa.gov/). Stepwise and detailed demagnetisation (both thermal [TH] and alternating field [AF]) was conducted in the paleomagnetic laboratory at the University of New Mexico (UNM) (Albuquerque) and at the Institute of Earth Sciences "Jaume Almera" (Consejo

Superior de Investigaciones Científicas-Universitat de Barcelona). TH demagnetisation was run with a TSD-1 furnace (Shonsted Ltd.), and remanent magnetization was measured with a 2G three-axis SQUID magnetometer in both laboratories. The 2G-AF demagnetizer was only used in the UNM laboratory.

Thermal stepwise demagnetisation used intervals of 50ºC between room temperature and 550-600ºC and AF increments between 3 and 10 mT up to 100mT (following an exponential trend) were run to characterize all paleomagnetic components of the NRM. Paleomagnetic directions were fitted by principal components analysis (PCA; Kirschvink, 1980) using the Paldir software by Utrecht Universiteit. In some cases, demagnetization circles (Bailey and Halls, 1978), the stacking routine (Scheepers and Zijderveld, 1992) and the virtual directions method (Ramón and Pueyo, 2017) were used to double-check the PCA results. Site means and terrace means were fitted by Fisher (1953) statistics. It is a probability distribution for multivariate directional data (vectors or simple lines in the 3D space.

3.2.3 Soil development

Soil development indices were used locally and regionally to correlate principal terrace levels (Lewis et al., 2009) and to estimate the age of the Qt3 terrace. Soils were described according to standard methods and nomenclature of the U.S. Soil Survey Staff (1993). Carbonate stage morphology follows nomenclature of Gile et al. (1981) and Birkeland (1999). Time-related changes in soil morphology were analyzed using a well-tested soil development index (SDI) (Harden, 1982; Harden and Taylor, 1983; McDonald et al., 1996) based on a soil chronofunction presented in Lewis et al. (2009).

SDI values were calculated using a conversion of soil morphologic properties (rubification, texture, structure, dry consistence, moist consistence, secondary carbonates, lightening, and argillans) into numerical data to enable a quantitative comparison of the degree of soil development. Horizon Development Index (HDI) values are obtained by normalizing each set of properties and a Profile Development Index (PDI) is calculated from HDI values and horizon thickness. The PDI values reflect the overall degree of soil development and provide a means of comparison among soils within a given sequence or area. The PDI has proven useful for providing correlations and calibrated age estimates for the sequence of strath terraces from the Cinca River valley (Lewis et al., 2009).

4. Results

4.1 Morphopedosedimentary characteristics of the staircase terrace sequence

The marked vertical separation between adjacent terraces, reinforced with extensive outcrops and their longitudinal continuity, facilitated mapping, regional correlation of terrace remnants, and descriptions of the fluvial terrace deposits along 170 km in the Cinca River valley (Figs. 3, 4).Ten paired staircase terraces (numbered Qt1, Qt2, Qt3, Qt4, Qt5, Qt6, Qt7, Qt8, Qt9, and Qt10, from oldest to youngest) have been preserved (Appendix 1). The terrace development and preservation are prominently displayed in the upper reach of the valley (near Ainsa, 50 km from the headwaters) and immediately downstream of the confluence with the Ara River (Figs. 3B, 4A, D). Mean height of the terrace straths above the active channel of the Cinca River in this sector are 172.5 m (Qt3), 44.2 m (Qt7) and 6.0 m (Qt9) (Table 1). The corresponding vertical

separations between adjacent preserved strath terraces are 128.3 m (Qt3-Qt7) and 38.2 m (Qt7-Qt9) respectively.

The lower reach of the valley goes from the External Pyrenees, where the Cinca River enters into the Ebro Basin, to the confluence with the Ebro River, including several important tributary junctions (the Esera, Vero and Alcanadre rivers). The lower reach shows the widest and best preserved terraces (Fig. 4B, E, F), particularly in the Albalate-Belver sector (125 km from the headwaters; Fig. 3C). Mean height of the terrace straths above the active channel of the Cinca River in this sector are 182.1 m (Qt1), 132.5 m (Qt2), 103.5 m (Qt3), 91.3 m (Qt4), 79.9 m (Qt5), 60.4 m (Qt6), 33.9 m (Qt7), 13.1 m (Qt8) and 3.6 m (Qt9) (Table 1). The corresponding vertical separations between adjacent strath terraces are 49.6 m (Qt1-Qt2), 29.0 m (Qt2-Qt3), 12.2 m (Qt3-Qt4), 11.4 m (Qt4-Qt5), 19.5 m (Qt5-Qt6), 26.5 m (Qt6-Qt7), 20.8 m (Qt7-Qt8) and 9.5 m (Qt8-Qt9).

Terraces Qt3, Qt7 and Qt9 are broadly preserved along the Cinca River valley (Appendix 1). Terraces older than Qt7 are preserved only on the river's east bank, indicating the westward migration of the Cinca River. This migration is well noted in the Albalate-Belver sector and reaches a lateral westward displacement of 8 km between Qt1 at Monte Julia and Qt7 at Albalate (Fig. 3C). Qt7 and subsequent Qt8 and Qt9 terraces outcrop in both sides of the valley. This implies a significant change in the width of the valley. In fact, Qt7 is approximately 5 km wide in the Albalate-Alcolea section, whereas the current valley bottom (active channel and floodplain) reaches a maximum width of 2 km (Fig. 3C).

Terrace treads are typically broad (2-4 km width) and commonly underlain by 2.8-7.7 m (Fig. 4C) of largely cobble-rich gravel with a sand-rich matrix, large (20-100 cm diameter) sub-rounded boulders, sparsely populated with sand lenses, and capped by either gravelly sand-rich alluvium or finer-textured overbank deposits. Fluvial deposits occur in fining-upwards sequences. According to lithofacies of Miall (1978), gravels are generally massive but locally imbricated (Gm) and cross-stratified (Gt, Gp), are well-sorted and sub-rounded and consist of limestone, sandstone, granite, quartzite, and schist (in order of decreasing abundance) of Pyrenean and, locally, Ebro basin provenances. Interbedded sand lenses can be cross-stratified (St, Sp) or horizontally laminated (Sh). Gravels can be capped by overbank silts (Fm).

Strath surfaces are carved into Cretaceous to Eocene marine carbonates and marls (Fig. 4A) along the river's Pyrenean reach and Eocene-Miocene continental deposits (Fig. 4B) along the Ebro Basin reach (Fig. 2B; Appendices 1 and 2). Localized deformation of the strath surface and associated gravels (e.g., tilting and faulting) occurs in places and is related to salt diapirism and gypsum dissolution confined to the Barbastro anticline and the Estada-Estadilla diapir (Sancho, 1988, 1989; Lucha et al., 2008) (Appendix 1). Local deformation related to small vertical faults was also observed near El Grado and El Pueyo de Araguás.

The Qt1 terrace is poorly preserved and only occurs between Albalate and Binaced (Figs. 3C, 4F; Appendix 1), where remnants occur as isolated hills (San Salvador and Las Brujas sites). The Qt1 remnants constitute the highest preserved remnants of the Cinca River terrace sequence. Mean thickness of alluvial cover is around 7.7 m and maximum grain size (Dmax) ranges from 30-48 cm (mean value 42±9 cm) (Appendix 2). An

eroded petrocalcic soil horizon (~1 m thick) formed in fine-grained sediments is preserved in places.

The Qt2 strath terrace is more or less continuously preserved between Albalate and Belver and is in the cicinity of the Qt1 remnants (Figs. 3C; Appendix 1). Mean thickness of alluvial cover preserved is around 5.6 m and maximum grain size (Dmax) ranges from 36-48 cm (mean value 41±4 cm) (Appendix 2). The soils found on the Qt2 are only weakly to moderately developed and are considerably less developed that the soils on the younger Qt3 terrace. This indicates that the original terrace surface has been severely eroded.

The Qt3 terrace is one of the two most important geomorphic features along the Cinca River valley. It is preserved continuously in the lower reach of the valley between Monzón and Fraga (Figs. 3C, 4F; Appendix 1); other relevant outcrops have been identified at Barbastro, El Grado and Ainsa (Figs. 3B, 4D; Appendix 1). Mean thickness of alluvial cover is around 5.8 m and maximum grain size (Dmax) ranges from 26-50 cm (mean value 34±6 cm) (Fig. 5; Appendix 2). Locally the Qt3 deposit near El Grado is faulted. Soil characteristics on this terrace are described below.

The Qt4 terrace is preserved only between Barbastro and Fraga (Figs. 3C, 4E; Appendix 1). Mean thickness of alluvial cover is around 5.2 m and maximum grain size (Dmax) ranges from 26-43 cm (mean value 35±8 cm) (Appendix 2). Near Belver, the terrace deposits include a 90 cm-thick aeolian cap that overlies 90 cm of overbank fines. An OSL date on the loess cap constrains its age to be 20±3 ka (Lewis et al., 2009), likely deposited during the MIS2 glaciation. No soils were described on the Qt4 terrace due

to surface erosion. In some localities, reworking of the Qt4 surface is evidenced by a cap of colluvium incorporating pieces of underlying petrocalcic horizons.

The Qt5 terrace is also preserved only between Monzón and Fraga Fraga (Fig. 3C; Appendix 1). Stratigraphic relations between the Qt4 and Qt5 terraces indicate that formation of the Qt5 terrace cannibalized much of the older Qt4 terrace. Mean thickness of alluvial cover is around 4.5 m and maximum grain size (Dmax) ranges from 28-51 cm (mean value 38±7 cm) (Appendix 2). North of Castejón del Puente, the Qt5 terrace was deformed by the diapiric activity of the Barbastro salt anticline (Sancho, 1989). The Qt5 soils in the Albalate sector have well developed Bk and Bkm horizons with stage III+ to IV+ carbonate morphology (Table 2) (Lewis et al., 2009).

The Qt6 terrace is also preserved only between Monzón and Fraga Fraga (Figs. 3C; Appendix 1) and exposures of the deposits are very limited because the degradation of the scarps. Mean thickness of alluvial cover is around 5.1 m and maximum grain size (Dmax) ranges from 24-80 cm (mean value 39±19 cm) (Appendix 2). Soils have a well-developed Btk horizon and stage III+ carbonate morphology (Table 2) (Lewis et al., 2009).

Remnants of the Qt7 terrace occur continuously along approximately 120 km of the Cinca valley (Figs. 3B, C, 4; Appendix 1). This is the best-preserved terrace on the Cinca and the most relevant terrace marker in the landscape. Terrace remnants are broad and up to 4 km in width along the lower reach. Mean thickness of alluvial cover is around 5 m. Maximum grain size (Dmax) ranges from 20-68 cm (mean value 34±9 cm) (Fig. 5; Appendix 2). Local distribution of terraces in the Albalate area suggests that

Qt7 terrace formation cannibalized much of older Qt6 and Qt5 terraces. In some locations, there is 3-4 m of colluvium on top of the Qt7 fluvial deposits. The Qt7 strath surface and overlying deposits are deformed when the underlying bedrock is composed of Upper Triassic evaporites and clays (Estada-Estadilla diapir) and Eocene evaporites (Barbastro salt anticline) (Sancho, 1989; Lucha et al., 2008). Local small faults deform the Qt7 deposits at El Pueyo de Araguás. The Qt7 soils in the Albalate sector have moderately to well-developed Btk horizons and stage II to weak stage III carbonate morphology (Table 2) (Lewis et al., 2009).

The Qt8 terrace is not as extensively preserved as Qt7; it crops out only along the lower 35 km of the valley (Fig. 3C; Appendix 1), where it is 2-3 km wide. Mean thickness of alluvial cover is around 2.7 m and maximum grain size (Dmax) ranges from 22-42 cm (mean value 29±6 cm) (Appendix 2). Soils in the Albalate sector have moderately developed Btk horizons with stage II carbonate morphology (Table 2) (Lewis et al., 2009).

The Qt9 terrace is generally co-extensive with the Qt7 terrace and traceable along 140 km of the total length of the river valley (Figs. 3B, C, 4D, E, F; Appendix 1). The Qt9 terrace is also largely co-extensive with Qt8, where the latter is preserved, and is approximately 2 km wide. Maximum grain size (Dmax) ranges from 12-60 cm (mean value 29±12 cm) (Fig. 5; Appendix 2) and mean thickness of alluvial cover is around 3.3 m. Locally this terrace is considerably thicker (e.g.,10 m at Castejón del Puente) because of deposition across the synsedimentary karstic subsidence on the south flank of the Barbastro salt anticline. The Qt9 soils in the Albalate sector have moderately

developed Bw and Bk horizons with stage I+ carbonate morphology (Table 2) (Lewis et al., 2009).

The Qt10 terrace (Figs. 3B, C, 4E, F), which is in an extensive active floodplain, has Roman bridge abutments preserved on its top near Castejón del Puente, demonstrating that this has been the active surface since at least Roman times in the region (from ca. 140 BC until ca. 400 AD, approximately about 2,000 years ago) (Beltrán, 1985).

4.2 Terrace profiles

The longitudinal profiles of the terrace straths and the active channel of the Cinca River were reconstructed (Fig. 6) from 300 GPS measurements (Appendices 1 and 2) and a few elevations derived from topographic maps. Strath heights (projected to a common vertical plane down the center of the modern stream valley) reveal several consistent patterns along the length of the Cinca River from headwaters to its confluence with the Ebro River. Several key features of the terrace profiles are significant.

First, the Cinca River has experienced progressive fluvial incision subsequent to formation of the Qt1 terrace, producing a marked vertical separation among terraces (Fig. 6; Table 1). As a consequence, a noticeable and well expressed staircase pattern has developed along the valley.

Second, overall longitudinal profiles are semi-parallel with a slight, but clear, upstream divergence (Fig. 6). The greatest expression of divergence is recorded by the Qt3 terrace with vertical separation between the active channel and strath surface ranging

from 165-175 near Ainsa (km 50), 130-135 m at Barbastro (km 100) and 95-105 m at Zaidín (km 155). Locally variable effects in divergence are observed along the profile due to rock resistance, active faulting, and gypsum diapirism and dissolution; however, these effects cannot explain the first-order longitudinal trends. The Qt7 profile also diverges upstream with respect to the active channel, although not as markedly. For example, the Qt7 is 45-50 m above the active channel near Ainsa, 40 m at Barbastro and 30-35 m near Zaidín.

The log plot of longitudinal profiles also shows changes in gradient at the Pyrenean mountain front. A prominent knickpoint occurs in the active channel at 90 km from the headwaters near El Grado (Fig. 6). This knickpoint is related to the higher erosional resistance of the folded rocks (Cretaceous and Eocene limestones) of the External Pyrenees (Fig. 2B; Appendix 1), as opposed to less resistant clastic sedimentary rocks at the margin of the Ebro basin. The knickpoint appears to be spatially fixed because its location has persisted through time for straths associated with Qt3, Qt7, Qt9 terraces and the active channel.

4.3 Terrace chronology

4.3.1 Geochronology for terraces Qt5 to Qt9

Numerical ages of the five youngest terraces (Qt5, Qt6, Qt7, Qt8, and Qt9) (Table 3) of the Cinca River sequence have been previously reported by Lewis et al. (2009), from multiple OSL dates and reinforced using regional soil stratigraphy. To summarize, Lewis et al. (2009) obtained two dates for Qt5 terrace (171 ± 22 ka and 180 ± 12 ka), giving a weighted mean age of 178 ± 21 ka, and one date for Qt6 (97 ± 16 ka). Six samples from

Qt7 terrace constitute a tightly grouped set of dates (63 ± 12, 59 ± 13, 64 ± 13, 61 ± 3, 56 ± 4 and 65 ± 5) with a weighted mean age of 61 ± 4 ka. Five dates on Qt8 terrace (39 ± 5, 42 ± 6, 47 ± 4, 50 ± 4 and 50 ± 3) gave a weighted mean age of 47 ± 4 ka. Finally, eight well grouped OSL dates for Qt9 terrace gave a weighted mean age of 11 ± 1 ka. The Qt7 terrace is correlated with glacial and fluvioglacial deposits in the Cinca headwaters (confluence of the Cinca and Cinqueta rivers at Mesón de Salinas) (Fig. 3A) that have a mean age of 64±11 ka, corresponding to the last maximum glacier extension in the south-central Pyrenees (Sancho et al., 2003). More detailed information from OSL measurements and derivation of mean terrace deposit dates is presented in Lewis et al. (2009).

4.3.2 Paleomagnetic data

The intensity of the NRM from terrace deposits of the Cinca River ranged in intensity from 0.132 to 317 mA/m with an average of 39.98 mA/m (±3.8 mA/m), although 90% of the data were between 0.4 and 200 mA/m (Fig. 7A). After spurious components at very low temperatures (below 200ºC), with occasional large intensities, stable paleomagnetic directions were observed between 250 ºC and 560-600 ºC in the thermal treatment (Fig. 7B). Alternating field treatment was not as successful in isolating stable directions, although some reliable directions (comparable to TH sister samples) were identified from 8-10 mT up to 40 mT (and even 80 mT; see for example samples 77a and 77b) (Fig. 7B). The primary and stable component of the magnetic field is characterized by low-coercivity and medium-temperature minerals pointing to magnetite as the main carrier of the magnetization.

Lower and intermediate terraces (from Qt9 to Qt3) unambiguously registered normal polarity of the primary paleomagnetic field (Fig. 7C). On the other hand, the high level Qt2 terrace unequivocally recorded a reversed polarity. This crucial observation is well supported by the consistent directions obtained in three different pits (T9-1, T9-2 and T9-3) in the Mombrún area (near Albalate) (Table 4). The oldest terrace (Qt1) recorded an intermediate pattern, displaying both polarities and scattered directions, although only one pit was sampled in this terrace. Paleomagnetic directions found in the Cinca terrace sequence, therefore, are consistent (equal demagnetization intervals and carriers), display pseudo-antipodal polarities (N: 355, 58 [α95: 10.6° and k: 5.7]; R: 220,-48 [α95: 20.6° and k: 5.74]) and seem to be a reliable record of the primary paleomagnetic field (Fig. 7C).

Despite individual paleomagnetic means that were weakly defined partially due to the small number of demagnetized samples (Table 4), the mean directions and polarities were consistent among the different samples sites across the same terrace. Besides, the stereographic projection merging all data together gives robust and speudo-antipodal means that allow us to be confident about the primary character of the magnetic record.

In view of these results, a relative chronology can be established (Table 1). All studied terraces younger than Qt3 display a normal polarity and belong to the Brunhes period in agreement with the available OSL dates for Qt5 to Qt9. The Qt2 terrace must belong to the Matuyama reverse period, likely close to the Brunhes/Matuyama reversal, and its boundary (C1r/C1n: 0.773 Ma) (Singer, 2014) must be located between the Qt3 and Qt2 terraces. The poor results found in the Qt1 terrace prevent the proposal of any

reliable interpretation, although they point to the occurrence of another zone with normal polarity. Future chronologic studies may shed light on interpretation and distinguish between Jaramillo and Cobb Mt. normal events. These two hypotheses have been recently proposed in other locations in the Ebro Basin (Sancho et al. 2016; Gil et al., in review).

4.3.4 Qt3 soil characteristics and estimated soil age

Soils formed on the Qt3 surfaces along the upper (Ainsa) and lower (Albalate) reaches of the Cinca River valley have the strongest degree of development relative to soils formed on the younger terraces (Table 2). Soils on the Qt3 terrace near Albalate vary in development, reflecting soils that have formed in either the original cobble-gravel bar deposits or in the original channel settings where the soil parent material consist of fine-textured overbank (with possible aeolian contributions) that overlies gravel-rich alluvium. Soils formed in depositional bars have weakly developed Btk horizons that overlie well-developed Bkm horizons with Stage IV to V carbonate morphology. Soils formed in channel settings have weak- to moderately-developed Btk horizons with stage IV carbonate morphology. Soil depth to the Bkm horizons ranges from 35 to 88 cm and occurs at a shallower depth for soils formed in bar deposits. Soil PDI (profile development index) values range from 61.4 to 80.8 for the Qt3 soils (Table 2).

By comparison, soils formed on the Qt3 terrace surface near Ainsa reflect soil formation under a much wetter subhumid climate. Soil development primarily consists of very thick soil Bt horizons with patchy to nearly continuous coatings of clay along pores, ped faces and gravels. B horizon thickness on the Qt3 surface exceeds 300 cm.

There is no carbonate accumulation in Qt3 terrace soils along the upper reach of the Rio Cinca valley due to the high effective soil moisture. The only soil described on the Qt3 surface near Ainsa has a PDI value of 105.1 (Table 2). The higher value reflects the greater degree of soil development that has occurred under the more humid climate at Ainsa sector relative to soils forming near the Albalate sector.

Soil age estimates for the Qt3 were based on the soil chronofunction developed by Lewis et al. (2009) and the PDI values calculated for the five soils described near Albalate. We did not include the Ainsa Qt3 soil because its more humid soil environment is not compatible with the soil chronofunction developed for soils in more arid settings. Soil age estimates (based on each PDI value; Table 2) ranged from 291 to 565 ka; mean age was 401±117 ka (Table 1). The Qt3 soils were better developed than soils formed on the Qt5 surface, which is aproximately 178 ka (Table 2).

4.4 Incision rates

River incision rates have been calculated by comparing the vertical separation (m) and the elapsed time (ka) between successive terrace strath surfaces. For this level of analysis, we considered that strath formation and the deposition of the corresponding alluvium are generally synchronous in time. The terrace sequences at Ainsa (kilometer 50 from headwaters; upper valley reach) and at Albalate (kilometer 125 from headwaters; lower valley reach) sectors (Fig. 6) were selected because of the extensive presence of well-preserved terrace remnants in both areas (Figs. 3B, C, 4D, F). Differential mean heights, elapsed mean time and mean incision rates for the selected

sets of coupled terraces are summarized in Table 5. Uncertainties in numerical dating were also considered to present maximum and minimum fluvial incision rates (Table 5).

Considering mean incisions from the coupled successions Qt3-Qt7, Qt7-Qt9 and Qt9-active channel, we proposed that a regional mean fluvial incision rate of 0.47 m ka^{-1} occurred during the Middle and Late Pleistocene. The spatial and temporal patterns of river incision also show some singularities. Rates of fluvial incision decreased downstream from Ainsa to Albalate; mean incision rates were 0.56 m ka^{-1} at Ainsa and 0.38 m ka^{-1} at Albalate. Additionally, the mean incision rate obtained from the coupled succession Qt3-Qt7 was 0.38 m ka^{-1} at Ainsa and 0.20 m ka^{-1} at Albalate (Table 5). For the coupled succession Qt7-Qt9, values were 0.76 m ka^{-1} and 0.61 m ka^{-1}, respectively. The coupled Qt9-active channel succession indicates incision of 0.54 m ka^{-1} at Ainsa and 0.33 m ka^{-1} at Albalate. These results clearly indicate that incision rates were higher on the upper reach relative to the lower reach over the considered time intervals.

The temporal pattern of variation in incision rates along the Cinca River valley reflects important changes during the Middle and Late Pleistocene. These changes are well observed in the Albalate sector, where the more complete sequence of terraces is preserved (Table 5). The Middle Pleistocene coupled Qt3-Qt5 terraces reflects an incision rate of 0.11 m ka^{-1}. By comparison, the incision rate of 0.24 m ka^{-1} was considerably higher during the Middle-Late Pleistocene transition for the coupled Qt5-Qt6 terraces. The Cinca River attained the highest incision rates during the Late Pleistocene. Pairing the Qt6-Qt7 terraces gives an incision rate of 0.74 m ka^{-1} and the

coupled Qt7-Qt8 terraces yields the maximum calculated rate of 1.48 m ka^{-1}. For the coupled Qt8-Qt9 terraces and the Qt9-Active channel, incision rates were substantially lower: 0.26 m ka^{-1} and 0.33 m ka^{-1}, respectively (Table 5; Fig. 8). Time-related trends in incision rates along the Ainsa sector, where the number of couples of terraces is less, were similar (Table 5; Fig. 8). As a consequence, the temporal incision pattern shows very low rates over the Middle Pleistocene, a gradual increase until the beginning of the Late Pleistocene (maximum rates at 60-50 ka) and then a gradual decrease to the present.

Additionally, taking into account the proposed paleomagnetic dates for Qt1 (Jaramillo event, 999-1070 ka) and Qt2 (reversed period previous Jaramillo event, 780-999 ka) in the Albalate sector (Table 1), we can tentatively estimate mean incision rates of 0.06 m ka^{-1} and 0.34 m ka^{-1} for the coupled terraces of Qt2-Qt3 and Qt1-Qt2, respectively (Table 5; Fig. 8).

5. Discussion

Landscape evolution and regional fluvial incision reflects an integration between uplift and climate (e.g., Whipple and Tucker, 1999; Gibbard and Lewin, 2009; Wegmann and Pazzaglia, 2009; Westaway et al., 2009; Stokes et al., 2012; Pazzaglia, 2013). Some studies have defined the geodynamic state (e.g., Lewis et al., 2000; Cloetingh et al., 2002; Garcia-Castellanos et al., 2003; Gunnell et al., 2008; Casas-Sainz and de Vicente, 2009; Fernández-Lozano et al., 2011) and the climate evolution based on fluvial records (Fuller et al., 1998; Lewis et al., 2009; Benito et al. 2010; García-Ruiz et al., 2013; Whitfield et al., 2013; Sancho et al., 2015) during the Quaternary in NE Spain.

The results presented above provide an opportunity to better understand the factors constraining regional and temporal fluvial incision patterns in the NE Iberian Peninsula.

5.1 Regional fluvial incision pattern

The regional pattern of the Cinca River incision can be basically defined by (i) the well-marked vertical separation between successive terrace straths, (ii) the near-parallel terrace strath profiles, and (iii) the westward migration of the Cinca River through time. The calculated mean river incision rate in the Cinca River valley (Pyrenees and Ebro Basin) during the Middle and Late Pleistocene was 0.47 m ka^{-1}. This rate is similar to channel incision rates of ≤ 1 m ka^{-1} for mountainous regions where commonly paired and extensive terraces occur (Wegmann and Pazzaglia, 2009). A maximum incision rate of 0.98 m ka^{-1} in the Miranda basin (Upper Ebro river valley), also within the Pyrenees, has been indicated by Soria-Jáuregui et al. (2016). Although regional data on river incision rates across the Iberian Peninsula are limited, the topographic pattern of river incision in the Pyrenees and the Ebro Basin is clearly different than those observed in the nearby Iberian Range (Giachetta et al., 2015) or in other extensive Iberian Tertiary basins drained by rivers flowing into the Atlantic Ocean. Mean fluvial incision rates of 0.065 m ka^{-1} from the terrace sequence of the Arlanzón River (Duero Basin) have been reported by Moreno et al. (2012), and a figure of 0.05 m ka^{-1} for terraces in different river valleys in the Central Tagus Basin has been roughly estimated by Silva et al. (2013, 2016). Fluvial incision rates of 0.07-1 m ka^{-1} (Cunha et al., 2005, 2008) and 0.13-0.53 m ka^{-1} (Martins et al., 2009) have been calculated from terrace sequences in the Lower Tagus River basin.

5.1.1 Vertical separation between strath terraces

In the Cinca River valley, vertical separation between couples of adjacent terrace straths ranged from approximately 10 to 50 m near Albalate (Table 5). Uplift must be sufficiently high to produce well marked altitudinal separation between terraces (Wang et al., 2015). He et al. (2015) obtained incision rates of 0.62-1.83 m ka^{-1} for terraces developed in rapidly uplifting mountainous areas (SE Tibetan Plateau), clearly higher than in the Cinca River valley under post-tectonic conditions. Many studies have demonstrated how long-term incision rates serve as a proxy for bedrock uplift rates (Merritts et al., 1994; Bridgland, 2000; Pazzaglia and Brandon, 2001; Wegmann and Pazzaglia, 2002; Bridgland and Westaway, 2008).

There are three regional geodynamic mechanisms that likely explain the geomorphic expression of the incision of the Cinca River. First, post-orogenic lithosphere uplift in the northeastern Iberian margin could be at least partially attributed to isostatic adjustment resulting from crustal thickening influenced by pre-existing faults (Casas-Sainz and de Vicente, 2009; Fernández-Lozano et al., 2011).

Second, lithosphere uplift could also be related to erosional unloading in the Pyrenees and the Ebro Basin after the connection of the drainage system with the Mediterranean Sea at the end of the Late Miocene (Coney et al., 1996; Vergés et al., 1998; Waltham et al., 2000; Garcia-Castellanos et al., 2003; Gibson et al., 2007; Stange et al., 2016; Garcia-Castellanos and Larrasoaña, 2015). Erosional denudation has prevailed for at least the last 10 Ma in the Central Pyrenees (Coney et al., 1996; Fitzgerald et al., 1999; Garcia-Castellanos et al., 2003; Gibson et al., 2007) and

thermochronologic (U-Th/He) data indicate uniformly low rates (0.2 mm/yr) (Gibson et al., 2007). On the other hand, it should be noted that the thickness of sedimentary fill in the north-central sector of the Ebro basin during the Late Oligocene and Early Miocene exceeded 5,000 m and consequently caused important flexural load effects on the lithosphere (Gaspar-Escribano et al., 2001). Considering the topography of the youngest Tertiary rocks (Pérez-Rivarés et al., 2002) preserved in the Central Ebro Basin (Monte Oscuro and San Caprasio, 812 m a.s.l.) and the altitude of the active Cinca channel close to the confluence into the Ebro River (Mequinenza Reservoir, 80 m a.s.l.), a denudation of 750 m must be considered as a minimum to explain the erosional rebound. The flexural isostatic compensation of the eroded materials from the Ebro basin is considered by Garcia-Castellanos and Larrasoaña (2015) to be the major force driving fluvial incision and topographic development.

A third factor that could also modulate Quaternary regional uplift required to develop the terrace sequence of the Cinca River is the occurrence of a warm, buoyant asthenosphere perhaps related to adjacent active crustal extension and volcanism in northeastern Spain (Lewis et al., 2000). This is further supported by Janssen et al. (1993) who presented a model of subsidence in the Valencia Trough and associated uplift in the eastern Iberian margin during the Pliocene. Mantle dynamics during post-orogenic stages may also account for the uplift in the Pyrenees and the Ebro southern foreland basin (Stange et al., 2016). However, Garcia-Castellanos and Larrasoaña (2015) considered forces related to mantle flow to have a minor role in building the post-tectonic topography of the Ebro basin.

Finally, although numerical dates to establish correlations are very limited, the broadly uniform altimetry of the staircase terrace sequences in the valleys of the main tributaries flowing into the Ebro River from the Pyrenees (Noguera Ribagorzana, Cinca, Alcanadre and Gállego rivers, from east to west) is noticeable (Gutiérrez and Peña, 1994).

5.1.2 Near-parallel strath profiles

In addition to vertical separation between terrace straths of the Cinca River, near-parallel concave-upward terrace profiles were also clearly demonstrated (Fig. 6). Steady regional crustal uplift would drive uniform fluvial incision and invariant incision rates, resulting in parallel terrace longitudinal profiles (Schlunegger and Hinderer, 2001; Pazzaglia, 2013). As a consequence, we postulate a trend to a uniform uplift rate over the Pleistocene in NE Iberia.

A weak trend upstream divergence of strath profiles was also observed. The upstream divergence among Qt3, Qt7 and Qt9 profiles includes a decrease in terrace gradient from Qt3 to Qt9 terraces (Fig. 6). The stream gradient controls both the stream-power and the transport capacity (Hack, 1973) through flow velocity. On the other hand, bedload movement by rolling is related to flow velocity near the streambed (Chorley et al., 1984). As a consequence, gravel-size transport is directly related to channel gradient. Considering the more representative strath terraces along the Cinca River valley (Qt3, Qt7 and Qt9), the maximum grain size (Dmax) (34±6 cm, 34±9 cm and 29±12 cm, respectively) remained near-uniform (Fig. 5). Then, flow velocity during deposition of the Qt3, Qt7 and Qt9 alluvium remained nearly uniform. Clast-size

averages of the entire set of terraces overlapped within uncertainties. A decrease in the maximum grain size (Dmax) along each terrace profile has also been observed (Fig. 5), which indicates that the hydraulic shear stress decreases proportionally to the gradient of the stream (Schumm, 1977; Larue, 2008; Pazzaglia, 2013).

The upstream divergence of terrace straths along the Cinca River indicates differential regional uplift as a primary driver of terrace formation rather than changes in fluvial erosivity and incision driven by cycles of climate transition (Whipple et al., 1999; Whipple and Tucker, 1999). Several mechanisms may be involved to explain the postulated differential regional uplift: (i) a reinforced uplift in response to a higher denudation rate affecting the Pyrenees as a function of topographic relief (Champagnac et al., 2008; Stange et al., 2016); (ii) an isostatic rebound of the Central Pyrenees related to lithospheric thickening (Zeyen and Fernández, 1994; Gunnel et al., 2008), supported by an important negative Bouguer anomaly associated with the Pyrenean building (Casas et al., 1997); and (iii) a flexural rebound related to removal of Pleistocene glaciers in the headwaters of the Cinca-Cinqueta valley (Belmonte, 2014).

5.1.3 Migration westward of the Cinca River

The Cinca River has markedly migrated to the west during incision, based on the distribution of mapped terrace surfaces (Fig. 3B, C; Appendix 1). The maximum lateral westward displacement reached 7 km between Qt3 and Qt7 in the Albalate section of the lower Cinca River valley. Westward migration ceased from the Qt7 terrace (61±4 ka). The observed arrangement of the terraces extends to the regional scale because it is common in the Pyrenean side of the central Ebro Basin, as has been shown in the

Noguera Ribagorzana River valley (Peña-Monné, 1983; Sancho, 1988), to the east of the Cinca River, in the Alcanadre River valley (Rodríguez, 1986; Calle et al., 2013), and the Gállego River valley (Benito, 1989), to the west of the Cinca River.

Lateral migration can play an important role in the river incision rates because it maintains an unconstrained width of the valley over time and, as a consequence, the obtained river incision rates could be comparable. Fluvial incision into bedrock is basically proportional to the stream power and inversely proportional to the channel width (Howard et al., 1994; Sklar and Dietrich, 1998; Brocard and van der Beek, 2006). Terrace treads of the Qt1 to Qt7 terraces consist of wide aggradational surfaces (Figs. 3B, C, 4; Appendix 1). For example, the Qt3 valley section is approximately a minimum of 5.5 km wide at Barbastro and the Qt7 valley width reaches a minimum of 4.5 km at Santa Lecina. Subsequent to formation of the Qt7 terrace, the river valley becomes narrower and the available width to accommodate subsequent terraces decreases (Qt8 and Qt9) to a maximum of 2 km between Monzón and Fraga. Considering the uniform lithology of the geological bedrock (Schanz and Montgomery, 2016), the higher erosivity from Qt7 to Qt9 (the pair Qt7-Qt8 yields a rate of 1.48 m ka^{-1}), therefore, could be, at least partially, related to restrictions imposed by valley width.

Channel migration and the related asymmetry of Pleistocene terraces may also be controlled by the regional westward tilt of Oligocene-Miocene bedrock in the Ebro basin. Strata dip gently westward (5° maximum) along the western margin of the Cinca River valley (Sancho, 1988). This regional tilting requires an uplift mechanism more active in eastern Iberia, with tilting related to the uplift of the rift shoulder (including the eastern Pyrenees, the Catalan Coastal Ranges and the adjacent Ebro Basin)

(Janssen et al., 1993; Casas-Sainz and de Vicente, 2009) accompanying the opening of the western Mediterranean margin during the Neogene (Roca and Desegaulx, 1992; Coney et al., 1996; Lewis et al., 2000). The uniform altimetry of the sequences of terraces in the main Pyrenean tributaries of the Ebro River, from east to west, however, suggests a cessation of differential uplift in the Mediterranean shoulder from at least the Mid Pleistocene. As a consequence, increased eastern uplift plays an indirect role in the westward migration of the Cinca River through the tilting bedrock.

5.2 Changes in incision rates over the last 1 Ma

Analysis of incision rates indicates that non-uniform river incision in the Cinca River valley has occurred over the last 1 Ma (Table 5; Fig. 8). Temporal changes in fluvial incision rates are particularly well established in the lower reach of the valley where the terrace sequence is preserved. Changes in river incision rates over time can be linked to changes in uplift rates (He et al., 2015; Ruszkiczay-Rüdiger et al., 2016) and/or climate driven changes in erosivity (e.g., Whipple et al., 1999; Schlunegger and Hinderer, 2001; Hartshorn et al., 2002; Zaprowski et al., 2005; Yang et al., 2011).

Using currently available data, there is no evidence of variability in the tectonic uplift rate of NE Iberia during the Mid-Late Pleistocene (Casas-Sainz and de Vicente, 2009; Fernández-Lozano et al., 2011); however, strong variability in climate has been well established, particularly during the Penultimate and the Last Glacial cycles at regional scale (Lewis et al., 2009; Sancho et al., 2015). Lewis et al. (2009) linked fluvial aggradation phases during the Mid-Late Pleistocene in the Cinca River valley with enhanced periods of glacier outwash that produced high discharges of water and

sediment yield down-stream along the valley. Therefore, a close correlation was established between alluvial deposition and cold stages: Qt5 correlates to MIS6, Qt6 to the MIS5b-5c transition, Qt7 to MIS4, Qt8 to the H5 event and Qt9 to the Younger Dryas period (Lewis et al., 2009). Periods of higher fluvial incision would be likely during interstadial stages with a lower sediment supply and greater water discharge activated by retreating glaciers. There is a broad agreement that correlates valley aggradation to cold climates and river incision to transitional and warm climates (e.g., Chorley et al., 1984; Fuller et al., 1998; Vandenberghe and Maddy, 2001; Macklin et al., 2002; Pan et al., 2003; Vandenberghe, 2003; Gao et al., 2008; Wegmann and Pazzaglia, 2009).

Regional incision also reflects cycles of variable glacial meltwater discharge over time as a function of the extension and retreat of the Cinca and Cinqueta valley glaciers. For example, the last maximum glacier advance in the Central Pyrenees was at 60-70 ka (MIS4) (Sancho et al., 2003; Lewis et al., 2009) and correlates well with the Qt7 terrace (Lewis et al., 2009), the most important geomorphological marker along the valley. The Cinca-Cinqueta glacier system reached a length of 25 km at this time. Subsequent glacier retreat would produce increased runoff that, in turn, would accelerate fluvial downcutting resulting in higher rates of river incision (Dethier, 2001). As result, the highest expected fluvial incision rates would occur during the timing of the couple Qt7-Qt8 (from 61±4 ka to 47±4 ka) following the last maximum glacier extension. In fact, this is the case; the incision rate was 1.48 m ka^{-1} in the lower reach of the Cinca River valley (Albalate sector). Nonetheless, the decrease in valley width after Qt7 formation

must also be considered to explain this high incision rate, as has been previously indicated.

The incision rates obtained between Qt6 (97±16 ka) and Qt7 (61±4 ka) formation (0.74 m ka^{-1}) and between Qt9 and the active channel (last 11±1 ka) (0.33 m ka^{-1}) are also remarkable. Significantly lower incision rates were deduced during the Mid-Pleistocene (e.g., 0.11 m ka^{-1} between Qt3 and Qt5 in the Albalate sector), resulting from less intense glacial pulses and/or higher valley width maintained as a consequence of the migration westward of the Cinca River. Our results do not well match the acceleration in river incision during the Mid-Pleistocene Revolution at the global scale (Bridgland and Westaway, 2008). Regardless, the general temporal pattern in the lower reach of the Cinca River valley (Albalate sector) can be extrapolated to the upper reach (Ainsa sector).

Finally, agreement between denudation and isostatic rebound must also be considered (Garcia-Castellanos and Lasarroaña, 2015). The increase in fluvial entrenchment would involve a lowering of the regional drainage and an increased denudation between Qt6 (97±16 ka) and Qt8 (47±4 ka), which in turn implies a higher erosional isostatic uplift during this period demonstrating a positive feedback loop (Finnegan et al., 2008; Westaway et al., 2009; Schlunegger et al., 2011).

6. Conclusions

Incision rates derived from the regional distribution of a well-preserved sequence of staircase terraces along 170 km in the Cinca River valley have been developed for the last 1 Ma in the Central Pyrenees and the adjacent Ebro basin (NE Iberia). The

sequence is composed of ten well separated terraces (from Qt1 to Qt10) formed under post-orogenic geodynamics and glacial/ interglacial climate conditions. Formation of this extensive paired cyclic terrace sequence was climatically controlled and required a significant regional uplift. Combined results from terrace mapping, height of terrace straths and profiles, and numerical ages of the alluvium overlying terrace straths allow analysis of the spatial and temporal river incision patterns and provides several interpretation of mechanisms involved:

1) Considering coupled successions of the more extensive terraces (Qt3-Qt7, Qt7-Qt9 and Qt9-active channel), the mean fluvial incision rate along the Cinca River during the Middle and Late Pleistocene was approximately around 0.47 m ka^{-1}. This incision rate was slightly greater in the upper reach of the valley (Ainsa sector) (0.56 m ka^{-1}) than in the lower reach (Albalate sector) (0.38 m ka^{-1}). In addition, the highest incision rate (1.48 m ka^{-1}) in the lower reach of the valley occurred during Qt7-Qt8 terrace formation (61-47 ka) and the lowest rate (0.11 m ka^{-1}) occurred during Qt3-Qt5 terrace formation (401-178 ka).

2) The spatial distribution of incision rates showed a near-uniform pattern of fluvial down-cutting along the Cinca River valley. Nearly parallel terrace profiles were driven by a near-uniform regional uplift activated by (i) tectonic uplift related to lithospheric thickening and (ii) isostatic rebound in response to regional denudation unloading, after the connection of the Ebro Basin with the Mediterranean Sea. Subtle upstream divergence of strath profiles appears to be governed by a differential increased uplift in the upper mountainous reach of the valley (Axial Pyrenees) rather than by a decrease in climate-driven erosivity with time.

3) Temporal incision rates show a non-uniform time pattern throughout the last 1 Ma. The highest incision rate (1.48 m ka^{-1}) occurred during Qt7-Qt8 terrace formation (61-47 ka). This highest rate appears to be related to a combination of (i) the high glacial meltwater discharge after the last maximum advance of the Pyrenean Cinca-Cinqueta glacier system and (ii) by the deactivation of migration westward of the Cinca River, favouring a lower width of the valley. Currently, the Cinca River is not in equilibrium and modern incision continues.

Incision rates calculated in the Ebro Basin draining to the Mediterranean Sea are much higher than rates for the Iberian rivers flowing into the Atlantic Ocean. Undoubtedly, the post-tectonic geodynamic setting of NE Iberia, the denudation triggered after the exorheism of the Ebro basin and the Pleistocene glacier evolution in the Pyrenees play a determinant role in explaining this difference in landscape evolution at the Iberian scale.

Additional regional studies of staircase terrace sequences are necessary to validate the proposed spatial and temporal patterns and to confirm the combined effect of uplift and climate on fluvial incision rates and the landscape evolution of NE Iberia.

7. Acknowledgments

This paper is a tribute to Dr. Claudia J. Lewis, who died prematurely when we were developing the manuscript. At the picture, Claudia guiding a field-trip to the Cinca River Valley included in the program of the V Spanish Geological Congress (2004). The paper collects much of the hard work performed cooperatively between 1998 and 2012. Research was funded by grants from the National Geographic Society, the

National Science Foundation (EAR-0088714), U.S. Army Research Office grants DAAD19-03-1-0159 and W911NF-09-1-0256, the Spanish Ministry of Education, and a Fulbright Senior Scholar grant to C. Lewis. We thank the Institute of Geophysics and Planetary Physics and Laboratory Directed Research and Development (LDRD) at Los Alamos National Laboratory for additional funding. The Desert Research Institute provided GPS equipment. Laboratory soil analyses were carried out at the Desert Research Institute. We thank John Geissman, Bet Beamud and Miguel Garcés for use of the paleomagnetic labs at the University of New Mexico (Albuquerque) and the Institute of Earth Sciences “Jaume Almera” CSIC-UB (Barcelona, Spain). We thank Marta Lopez for combining all of our data into a Geographic Information System. This study is a contribution of the PALEOQ Research Group (Aragon Government and European Social Fund) and IUCA (University of Zaragoza). Authors thank two anonymous reviewers for their comments that helped improve the manuscript. Thanks are also due to the Editor Prof. Andy Plater for the final refinement of the manuscript.

References

Antón, L., Rodés, A., De Vicente, G., Pallàs, R, Garcia-Castellanos, D., Stuart, F.M., Braucher, R. and Bourlès, D. (2012). Quantification of fluvial incision in the Duero Basin (NW Iberia) from longitudinal profile analysis and terrestrial cosmogenic nuclide concentrations. Geomorphology, 165-166, 50-61.

Bailey, R.C. and Halls, H.C. (1984). Estimate of confidence in paleomagnetic directions derived from mixed remagnetization circle and direct observational data. Journal of Geophysics, 54, 174-182.

Barnolas, A., Gil-Peña, I. and Martín-Alfageme, S. (2009). Mapa Geológico de Pirineos a escala 1:400.000. IGME-BRGM.

Belmonte, A. (2014). Geomorfología del Macizo de Cotiella (Pirineo oscense): Cartografía, evolución paleoambiental y dinámica actual. PhD thesis, University of Zaragoza, 580 p.

Beltrán, A. (1985). Historia de Aragón, vol. II. Guara Editorial, 183 p. Zaragoza.

Benito, G. (1989). Geomorfología de la Cuenca Baja del río Gállego. PhD thesis, University of Zaragoza, 764 p.

Benito, G., Sancho, C., Peña, J.L., Machado, M.J. and Rhodes, E.J. (2010). Large-scale karst subsidence and accelerated fluvial aggradation during MIS6 in NE Spain: climatic and paleohydrological implications. Quaternary Science Reviews, 29, 2694-2704.

Birkeland, P.W. (1999). Soils and Geomorphology. Oxford University Press, New York. 430 p.

Bridgland, D.R. (2000). River terrace systems in north-west Europe: an archive of environmental change, uplift and early human occupation. Quaternary Science Reviews, 19, 1293-1303.

Bridgland, D. and Westaway, R. (2008). Climatically controlled river terrace staircases: A worldwide Quaternary phenomenon. Geomorphology , 98, 285-315.

Brocard, G.Y. and van der Beek, P.A. (2006). Influence of incision rate, rock strength, and bedload supply on bedrock river gradients and valley-flat widths: field-based

evidence and calibrations from western Alpine rivers (southeast France). In Willet, S.D., Hovious, N., Brandon, M.T. and Fisher, D.M. (Eds.). Tectonics, Climate and Landscape Evolution. Geological Society of America, Special Paper 398, 101-126.

Bull, W.B. (1991). Geomorphic Response to Climatic Change. Oxford University Press, 326 p. New York.

Burbank, D.W. and Anderson, R.S. (2001). Tectonic Geomorphology. Blackwell, 274 Malden.

Calle, M., Sancho, C., Peña, J.L., Cunha, P., Oliva-Urcia, B. and Pueyo, E. (2013). La secuencia de terrazas cuaternarias del río Alcanadre (provincia de Huesca): caracterización y consideraciones paleoambientales. Cuadernos de Investigación Geográfica, 39, 159-178.

Casas, A., Kearey, P., Rivero, L. and Adam, C.R. (1997). Gravity anomaly map of the Pyrenean region and a comparison of the deep geological structure of the western and eastern Pyrenees. Earth and Planetary Science Letters, 150, 65-78.

Casas-Sainz, A.M. and de Vicente, G. (2009). On the tectonic origin of Iberian topography. Tectonophysics, 474, 214-235.

Champagnac, J.D., van der Beek, P., Diraison, G. and Dauphin, S. (2008). Flexural isostatic response of the Alps to increased Quaternary erosion recorded by foleland basin remnants, SE France. Terra Nova, 20, 213-220.

Chorley, R.J., Schumm, S.A. and Sugden, D.E. (1984). Geomorphology. Methuen, 605 p. London.

Cloetingh, S. and Willett, S.D. (2013). TOPO-EUROPE: Understanding of the coupling between the deep Earth and continental topography. Tectonophysics, 602, 1-14.

Cloetingh, S., Burov, E., Beekman, F., Andeweg, B., Andriessen, P.A.M., Garcia-Castellanos, D., de Vicente, G. and Vegas, R. (2002). Lithospheric folding in Iberia. Tectonics, 21, 5-1–5-26.

Coney, P.J., Muñoz, J.A., McClay, K.R. and Evenchick, C.A. (1996). Syntectonic burial and post-tectonic exhumation of the southern Pyrenees foreland fold-and-thrust belt. Journal of the Geological Society, London, 153, 9-16.

Costa, E., Garcés, M., López-Blanco, M., Beamud, E., Gómez-Paccard, M. and Larrasoaña, J.C. (2010). Closing and continentalization of the South Pyrenean foreland basin (NE Spain): magnetochronological constraints. Basin Research, 26, 904-917.

Cunha, P.P., Martins, A.A., Daveau, S., Friend, P. (2005). Tectonic control of the Tejo river fluvial incision during the late Cenozoic, in Ródão-central Portugal (Atlantic Iberian border). Geomorphology, 64, 271-298.

Cunha, P.P., Martins, A.A., Huot, S., Murray, A.S. and Raposo, L. (2008). Dating the Tejo river lower terraces in the Ródão area (Portugal) to assess the role of tectonics and uplift. Geomorphology, 102, 43-54.

Cunha, P.P., Almeida, N., Aubry, T., Martins, A.A., Murray, S.A., Buylaert, J.P., Sohbati, R., Raposo, L. and Rocha, L. (2012). Records of human occupation from Pleistocene river terrace and aeolian sediments in the Arneiro depression (Lower Tejo River, central eastern Portugal). Geomorphology, 165-166, 78-90.

Dethier, D.P. (2001). Pleistocene incision rates in the western United States calibrated using lava Creek B tephra. Geology, 29, 783-786.

Dubar, M. and Semah, F. (1986). Paleomagnetic data bearing on the age of high terrace deposits (Durance Sequence) in Alpine valleys of southeastern France. Quaternary Research, 25, 387-391.

Duval, M., Sancho, C., Calle, M., Guilarte, V. and Peña-Monné, J.L. (2015). On the potential of the ESR dating method applied to optically bleached quartz grains in sedimentary fluvial environments: some examples from the Early Pleistocene terraces of the Alcanadre river (Ebro basin, Spain). Quaternary Geochronology, 29, 58-69.

Fernández-Lozano, J., Sokoutis, D., Willingshofer, E., Muñoz-Martín, A., De Vicente, G. and Cloetingh, S., (2011). Análisis integrado de la topografía y anomalías gravimétricas en la Península Ibérica: nuevas metodologías en modelación análoga. Revista de la Sociedad Geológica de España, 24, 153-171.

Finnegan, N.J., Hallet, B., Montgomery, D.R., Zeitler, P.K., Stone, J.O., Anders, A.M. and Yuping, L. (2008). Coupling of rock uplift and river incision in the Namche Barwa-Gyala Peri massif, Tibet. Geological Society of America Bulletin, 120, 142-155.

Fisher, R. (1953). Dispersion on a sphere. Proceedings of the Royal Society of London. Series A. Mathematical and Physical Sciences, 217, 295-305.

Fitzgerald, P.G., Muñoz, J.A., Coney, P.J. and Baldwin, S.L. (1999). Asymmetric exhumation across the Pyrenean orogen: implications for the tectonic evolution of a collisional orogen. Earth and Planetary Science Letters, 173, 157-170.

Fuller, I.C., Macklin, M.G., Lewin, J., Passmore, D.G. and Wintle, A.G. (1998). River response to high-frequency climate oscillations in southern Europe over the past 200 k.y. Geology, 26, 275-278.

Gao, H., Liu, X., Pan, B., Wang, Y., Yu, Y. and Li, J. (2008). Stream response to Quaternary tectonic and climatic change: Evidence from the upper Weihe River, central China. Quaternary Internacional, 186,123-131.

Garcia-Castellanos, D., Vergés, J., Gaspar-Escribano, J. and Cloetingh, S. (2003). Interplay between tectonics, climate, and fluvial transport during the Cenozoic evolution of the Ebro Basin (NE Iberia). Journal of Geophysical Research, 108, 2347, doi:10.1029/2002JB002073.

Garcia-Castellanos, D. and Larrasoaña, J.C. (2015). Quantifying the post-tectonic topographic evolution of closed basins: The Ebro basin (northeast Iberia). Geology, 43,663-666.

García-Ruiz, J.M., Martí-Bono, C., Peña-Monné, J.L., Sancho, C., Rhodes, E.J., Valero-Garcés, B., González-Sampériz, P. and Moreno, A. (2013). Glacial and fluvial deposits in the Aragón Valley, central-western Pyrenees: chronology of the Pyrenean late Pleistocene glaciers. Geografiska Annaler: Series A, Physical Geography, 95, 15-32.

Gaspar-Escribano, J. M., van Wees, J. D., ter Voorde, M., Cloetingh, S., Roca, E., Cabrera, L., Muñoz, J. A., Ziegler, P. A. and Garcia-Castellanos, D. (2001). Three-dimensional flexural modelling of the Ebro Basin (NE Iberia). Geophysical Journal International, 145, 349-367.

Giachetta, E., Molin, P., Scotti, V.N. and Faccena, C. (2015). Plio-Quaternary uplift of the Iberian Chanin (central-eastern Spain) from landscape evolution experiments and river profile modeling. Geomorphology, 246, 48-67.

Gibbard, P. and Cohen, K.M. (2008). Global chronostratigraphical correlation table for the last 2.7 million years. Episodes, 31, 243-247.

Gibbard, P.L. and Lewin, J. (2009). River incision and terrace formation in the late Cenozoic of Europe. Tectonophysics 474, 41–55.

Gibson, M., Sinclair, H.D., Lynn, G.J. and Stuart, F.M. (2007). Late- to post-orogenic exhumation of the Central Pyrenees revealed through combined thermochronological data and modeling. Basin Research, 19, 323–334.

Gil Garbi, H, 2017. Los depósitos cuaternarios en el sector central de la Cuenca del Ebro: Arquitectura sedimentaria, paleokarst, su interacción con la sedimentación y cronología. PhD thesis, University of Zaragoza, 354 p.

Gil, H., Luzón, A., Soriano, M.A., Casado, I., Pérez, A., Yuste, A., Pueyo, E.L. and Pocoví, A. (2013). Stratigraphic architecture of alluvial–aeolian systems developed on active karst terrains: an Early Pleistocene example from the Ebro Basin (NE Spain). Sedimentary Geology, 296, 122-141.

Gile, L.H., Hawley, J.H.and Grossman, R.B. (1981). Soils and geomorphology in the basin and range area of Southern New Mexico-guidebook to the desert project. New Mexico Bureau of Mines and Mineral Resources, Socorro, NM. Memoir 39, 222 p.

Gunnell, Y., Zeyen, H. and Calvet, M. (2008). Geophysical evidence of a missing lithospheric root beneath the Eastern Pyrenees: Consequences for post-orogenic uplift and associated geomorphic signatures. Earth and Planetary Science Letters, 276, 302-313.

Gutiérrez, M. and Peña, J.L. (1994). Depresión del Ebro. In Gutiérrez, M. (Ed.). Geomorfología de España, 305-349. Ed. Rueda. Madrid.

Hack, J.T. (1973). Stream-profile analysis and stream-gradient index. Journal Research U.S. Geological Survey, 1, 421-429.

Harden, J.W. (1982). A quantitative index of soil development from field descriptions: examples from a soil chronosequence in central California. Geoderma, 28, 1-28.

Harden, J.W. and Taylor, E.M. (1983). A quantitative comparison of soil development in four climatic regimes. Quaternary Research, 20, 342-359.

Hartshorn, K., Hovius, N., Dade, W.B. and Slingerland, R.L. (2002). Climate-driven bedrock incision in an active mountain belt. Science, 297, 2036-2038.

He, Z., Zhang, X., Bao, S., Qiao, Y., Sheng, Y., Liu, X., He, X., Yang, X., Zhao, J., Liu, R. and Lu, C. (2015). Multiple climatic cycles imprinted on regional uplift-controlled fluvial terraces in the lower Yalong River and Anning River, SE Tibetan Plateau. Geomorphology, 250, 95-112.

Howard, A.D., Dietrich, W.E. and Seidl, M.A. (1994). Modeling fluvial erosion on regional to continental scales. Journal of Geophysical Research 99 (B7), 13,971-13,986.

Jacobson, R.B., Elston, D. P. and Heaton, J.W. (1988). Stratigraphy and magnetic polarity of the high terrace remnants in the upper Ohio and Monongahela rivers in West Virginia, Pennsylvania, and Ohio. Quaternary Research, 29, 216-232.

Janssen, M.E., Torné, M., Cloetingh, S. and Banda, E. (1993). Pliocene uplift of the eastern Iberian margin: inferences from quantitative modelling of the Valencia Trough. Earth and Planetary Science Letters, 119, 585-597.

Kirschvink, J.L. (1980). The least-squares line and plane and the analysis of palaeomagnetic data. Geophysical Journal of the Royal Astronomical Society, 62, 699-718.

Larue, J.P. (2008). Tectonic influence on the Quaternary drainage evolution on the northwestern margin of the French Central Massif: the Cruese valley example. Geomorphology, 93, 398-420.

Lewis, C., McDonald, E., Sancho, C., Peña, J.L. and Rhodes, E. (2009). Climatic implications of correlated Upper Pleistocene glacial and fluvial deposits on the Cinca and Gállego Rivers (NE Spain) based on OSL dating ans soil stratigraphy. Global and Planetary Change, 67, 141-152.

Lewis, C.J., Vergés, J. and Marzo, M. (2000). High mountains in a zone of extended crust: Insights into the Neogene-Quaternary topographic development of northeastern Iberia. Tectonics, 19, 86-102.

Li, J.J., Fang, X.M., van der Voo, R., Zhu, J.J., Mac Niocaill, C., Ono, Y., Pan, B.T., Zhong, W., Wang, J.L., Sasaki, T., Zhang, Y.T, Cao, J.X., Kang, S.C. and Wang, J.M. (1997).

Magnetostratigraphic dating of river terraces: Rapid and intermittent incision by the Yellow River of the northeastern margin of the Tibetan Plateau during the Quaternary. Journal of Geophysical Research, 102, 10121-10132.

Lucha, P., Gutiérrez, F. and Guerrero, J. (2008). Environmental problems and geological implications derived from evaporite dissolution in the Barbastro salt anticline (NE Spain). Environmental Geology, 53, 1045-1055.

Macklin, M.G., Fuller, I.C., Lewin, J., Maas, G.S., Passmore, D.G., Rose, J.,Woodward, J.C., Black, S., Hamlin, R.H.B. and Rowan, J.S. (2002). Correlation of fluvial sequences in the Mediterranean basin over the last 200 ka and their relationship to climate change. Quaternary Science Reviews, 21, 1633-1641.

Martínez-Peña, M. and Casas-Sainz, A. (2003). Cretaceous-Tertiary tectonic inversion of the Cotiella Basin (southern Pyrenees, Spain). International Journal of Earth Sciences, 92, 99-113.

Martínez-Peña, B., Casas-Sainz, A. and Millán-Garrido, H. (1995). Palaeostresses associated with thrust sheet emplacement and related holding folding in the southern central Pyrennes, Huesca, Spain. Journal of the Geological Society, London, 152, 353-364.

Martins, A.A., Cunha, P.P., Huot, S., Murray, A.S. and Buylaert, J.P. (2009). Geomorphological correlation of the tectonically displaced Tejo River terraces (Gavião–Chamusca area, central Portugal) supported by luminescence dating. Quaternary International, 199, 75-91.

Martins, A.A., Cunha, P.P., Buylaert, J.P., Huot, S., Murray, A.S., Dinis, P., Stokes, M. (2010). K-feldspar IRSL dating of a Pleistocene river terrace sequence of the Lower Tejo River (Portugal, western Iberia). Quaternary Geochronology, 5, 176-180.

McDonald, E.V., Reneau, S.L. and Gardner, J.N. (1996). Soil-forming processes on the Pajarito Plateau: Investigation of a soil chronosequence in Rendija Canyon. In: Goff, F., Kues, B.S., Rogers, M.A., McFadden, L.D. and Gardner, J.N. (Eds.), New Mexico Geological Society Guidebook, 47th Conference. Socorro, New Mexico, USA, p. 375-382.

Merritts, J., Vicent, R. and Wohl, E. (1994). Long river profiles, tectonism and eustasy: a guide to interpreting fluvial terraces. Journal of Geophysical Research 99 (B7), 14031-14050.

Miall, A.D. (1978). Lithofacies types and vertical profile models in braided river deposits: a summary. In: Miall, A.D. (Ed.). Fluvial sedimentology. Canadian Society of Petroleum Geologists, Memoir 5, 597-604.

Moreno, D., Falguères, C., Pérez-González, A., Duval, M., Voinchet, P., Benito-Calvo, A., Ortega, A.I., Bahain, J.J., Sala, R., Carbonell, E., Bermúdez de Castro, J.M. and Arsuaga, J.L. (2012). ESR chronology of alluvial deposits in the Arlanzón valley (Atapuerca, Spain): Contemporaneity with Atapuerca Gran Dolina site. Quaternary Geochronology, 10, 418-423.

Muñoz, J.A. (2002). The Pyrenees. In Gibbons, W. and Moreno, M.T. (Eds.). The Geology of Spain, 370-385. Geological Society, London.

Muñoz, A., Arenas, C., González, A., Luzón, A., Pardo, G., Pérez, A. and Villena, J. (2002). Ebro basin (northeastern Spain). In Gibbons, W. and Moreno, M.T. (Eds.). The Geology of Spain, 301-309. Geological Society, London.

Pan, B.T., Burbank, D., Wang, Y.X., Wu, G.J., Li, J.J. and Guan, Q.Y. (2003). A 900 ka record of strath terrace formation during glacial-interglacial transitions in northwest China. Geology, 31, 957-960.

Pazzaglia, F.J. (2013). Fluvial Terraces. In Wohl, E. (Ed.). Treatise of Geomorphology, Volume 9, 379-412. Elsevier.

Pazzaglia, F.J. and Brandon, M.T. (2001). A fluvial record of rock uplift and shortening across the Cascadia forearc high. American Journal of Science, 301, 385-431.

Peña-Monné, J.L. (1983). La Conca de Tremp y Sierras Prepirenaicas comprendidas entre los ríos Segre y Noguera Ribagorzana: estudio geomorfológico. Instituto de Estudios Ilerdenses, 373 p., Lleida.

Peña-Monné, J.L. (1994). Cordillera Pirenaica. In Gutiérrez, M. (Ed.). Geomorfología de España, 159-225. Rueda, Madrid.

Pérez-Rivarés, J., Garcés, M., Arenas, C. and Pardo, G. (2002). Magnetocronología de la sucesión Miocena de la Sierra de Alcubierre (sector central de la Cuenca del Ebro). Revista Sociedad Geológica de España, 15, 3-4.

Pevzner, M.A. (1970). Paleomagnetic studies of Pliocene-Quaternary deposits of Pridniestrovie. Palaeogeography, Palaeoclimatology, Palaeoecology, 8, 215-219.

Pueyo, E.L., Garcés, M., Mauritsch, H.J., Lewis, C., Scholger, R., Sancho, C., Molina, R., Schnepp, E., Larrasoaña, J.C., Parés, J.M., Pocoví, A., Muñoz, A., Valero, B., Millán, H., Laplana, C., Oliva, B. and González, P. (2006). Sampling, transportation and magnetic-free consolidation of extremely soft sediments for paleomagnetic purposes: a successful “recipe”. In Calvo, M., Garcés, M., Gomes, C., Larrasoaña, J.C., Puedo, E. and Villalaín, J.J. (Eds). MAGIBER I: Paleomagnetismo en la Península Ibérica, 121-128. Universidad de Burgos, ISBN: 84-96394-35-2.

Puigdefábregas, C. and Souquet, P. (1986). Tecto-sedimentary cycles and depositional sequences of the Mesozoic and Tertiary from the Pyrenees. In Banda, E. and Wickham, S.M. (Eds.). The Geological Evolution of the Pyrenees, Tectonophysics, 129, 173-203.

Ramón, M.J., Pueyo, E.L., Oliva-Urcia, B. and Larrasoaña, J.C. (2017). Virtual Directions in Paleomagnetism: A Global and Rapid Approach to Evaluate the NRM Components. Frontiers of Earth Science, 5, 1-14.

Roca, E. and Desegaulx, P. (1992). Analysis of the geological evolution and vertical movements in the València trough area, western Mediterranean. Marine and Petroleum Geology, 9, 167-185.

Rodríguez, J. (1986). Geomorfología de las Sierras Exteriores oscenses y su piedemonte. Instituto de Estudios Altoaragoneses, Huesca, 172 p.

Ruskiczay-Rüdiger, Z., Braucher, R., Novothny, A., Csillag, G., Fodor, L., Molnár, G., Madarász, B. and ASTER Team (2016). Tectonic and climatic control on terrace formation: Coupling in sity produced 10Be depth profiles and luminescence approach, Danube River, Hungary, Central Europe. Quaternary Science Reviews, 131, 127-147.

Sancho, C. (1988). Geomorfología de la cuenca baja del río Cinca. PhD thesis, University of Zaragoza, 743 p.

Sancho, C. (1989). Deformaciones asociadas a la actividad diapírica cuaternaria del Anticlinal de Barbastro (provincia de Huesca). Cuaternario y Geomorfología, 3, 35-43.

Sancho, C., Calle, M., Peña-Monné, J.L., Duval, M., Oliva-Urcia, B., Pueyo, E.L., Benito, G. and Moreno, A. (2016). Dating the earliest Pleistocene alluvial terrace of the Alcanadre River: Insights on the landscape evolution of the Ebro Basin (NE Spain). Quaternary International, 407, 86-95.

Sancho, C., Peña, J.L., Lewis, C., McDonald, E. and Rhodes, E. (2003). Preliminary dating of glacial and fluvial deposits in the Cinca River Valley (NE Spain): chronological evidences for the Glacial Maximum in the Pyrenees?. In Ruiz, M.B., Dorado, M., Valdeolmillos, A., Gil, M.J., Bardají, T., Bustamante, I. and Martínez, I. (Eds.). Quaternary climatic changes and environmental crises in the Mediterranean region, 169-173. Universidad de Alcalá-Ministerio de Ciencia y Tecnología-INQUA.

Sancho, C., Arenas, C., Vázquez-Urbez, M., Pardo, G., Lozano, M.V., Peña-Monné, J.L., Hellstrom, J., Ortiz, J.E., Osácar, M.C., Auqué, L. and Torres, T. (2015). Climatic implications of the Quaternary fluvial tufa record in the NE Iberian Peninsula over the last 500 ka. Quaternary Research, 84, 398-414.

Santisteban, J. I. and Schulte, L. (2007). Fluvial networks of the Iberian Peninsula: a chronological framework. Quaternary Science Reviews, 26, 2738-2757.

Schanz, S.A. and Montgomery, D.R. (2016). Lithologic controls on valley width and strath terrace formation. Geomorphology, 258, 58-68.

Scheepers, P.J.J. and Zijderveld, J.D.A. (1992). Stacking in Paleomagnetism: Application to marine sediments with weak NRM, Geophysical Research Letters, 19, 1519-1522.

Schlunegger, F. and Hinderer, M. (2001). Crustal uplift in the Alps: why the drainage pattern matters. Terra Nova, 13, 425-432.

Schlunegger, F., Norton, K.P. and Zeilinger, G. (2011). Climatic forcing on channel profiles in the Eastern Cordillera on the Coroico region, Bolivia. The Journal of Geology, 119, 97-107.

Schumm, S.A. (1977). The fluvial system. John Wiley & Sons, 338 p. New York.

Scotti, V.N., Molin, P., Faccenna, C., Soligo, M. and Casas-Sainz, A. (2014). The influence of surfface and tectonic processes on landscape evolution of the Iberian Chain (Spain): quantitative geomorphological analysis and geochronology. Geomorphology, 206, 37-57.

Sklar, L. and Dietrich, W.E. (1998). River longitudinal profiles and bedrock incision models: stream power and the influence of sediment supply. In: Tinkler, K.J. and Wohl, E.E. (Eds.). Rivers Over Rock: Fluvial Processes in Bedrock Channels. Geophysical Monograph, 107. American Geophysical Union, 237-260. Washington D.C.

Silva, P.G., Roquero, E., López-Recio, M., Huerta, P. and Tapias, F. (2013). Statistical approach to the chronosequence of fluvial terraces in the Tagus and Duero basins

(Central Spain). In: Baena, R., Fernández, J.J. and Guerrero, I. (Eds.). El Cuaternario Ibérico: Investigación en el S. XXI, 29-33. Sevilla.

Silva, P.G., Roquero, E., López-Recio, M., Huerta, P. and Martínez-Graña, A.M. (2016). Chronology of fluvial terrace sequences for large Atlantic rivers in the Iberian Peninsula (Upper Tagus and Duero drainage basins, Central Spain). Quaternary Science Reviews doi.org/10.1016/j.quascirev.2016.05.027.

Singer, B.S. (2014). A Quaternary geomagnetic instability time scale. Quaternary Geochronology, 21, 29-52.

Soria-Jáuregui, A., González-Amuchástegui, M.J., Mauz, B. and Lang, A. (2016). Dynamics of Mediterranean late Quaternary fluvial activity: An example from the River Ebro (north Iberian Peninsula). Geomorphology, 268, 110-122.

Stange, K.M., van Balen, R., Vandenberghe, J., Peña, J.L. and Sancho, C. (2013). External controls on Quaternary fluvial incision and terrace formation at the Segre River, Southern Pyrenees. Tectonophysics, 602, 316-331.

Stange, K.M., van Balen, R.T., Garcia-Castellanos, D., Cloetingh, S. (2016). Numerical modelling of Quaternary terrace staircase formation in the Ebro foreland basin, southern Pyrenees, NE Iberia. Basin Research, 28, 124-146.

Starkel, L. (2003). Climatically controlled terraces in uplifting mountain areas. Quaternary Science Reviews, 22, 2189-2198.

Stokes, M., Cunha, P.P. and Martins, A. (2012). Techniques for analysing Late Cenozoic river terrace sequences. Geomorphology, 165, 1-6.

U.S. Soil Survey Staff (1993). Examination and description of soils. Soil Conservation Service. Soil survey manual. U.S. Department of Agriculture Handbook 18. Washington, D.C., USA, Chapter 3.

Vandenberghe, J. (2003). Climate forcing of fluvial system development: an evolution of ideas. Quaternary Science Reviews, 22, 2053-2060.

Vandenberghe, J. and Maddy, D. (2001). The response of river systems to climate change. Quaternary International, 79, 1-3.

Vergés, J., Marzo, M., Santaeulària, T., Serra-Kiel, J., Burbank, D. W., Muñoz, J. A. and Giménez-Montsant, J. (1998). Quantified vertical motions and tectonic evolution of the SE Pyrenean foreland basin. In: Mascle, A., Puigdefàbregas, C., Luterbacher, H.P. and Fernàndez, M. (Eds.). Cenozoic Foreland Basins of Western Europe, London, Geological Society Special Publications, 134, p. 107-134.

Viveen, W., Schoorl, J.M., Veldkamp, A. and van Balen, R.T. (2014). Modelling the impact of regional uplift and local tectonics on fluvial terrace preservation. Geomorphology, 210, 119-135.

Waltham, D.C., Docherty, C., Taberner, C. (2000). Decoupled flexure in the South Pyrenean foreland. J. Geophys. Res., 105, 16,329-16,340.

Wang, X., Vandenberghe, J., Shuangwen, Y., Van Balen, R. and Lu, H. (2015). Climate-dependent fluvial architecture and processes on a suborbital timescale in areas of rapid tectonic uplift: An example from the NE Tibetan Plateau. Global and Planetary Change, 133, 318-329.

Wegmann, K.W. and Pazzaglia, F.J. (2009). Late Quaternary fluvial terraces of the Romagna and Marche Apennines, Italy: Climatic, lithologic, and tectonic controls on terrace genesis in an active orogen. Quaternary Science Reviews, 28, 137-165.

Westaway, R., Bridgland, D.R., Sinha, R. and Demir, T. (2009). Fluvial sequences as evidence for landscape and climatic evolution in the Late Cenozoic: a synthesis of data from IGCP 518. Global and Planetary Change, 68, 237-253.

Whipple, K. and Tucker, G. (1999). Dynamics of the stream-power river incision model: Implications for height limits of mountain ranges, landscape response timescales, and research needs. Journal of Geophysical Research, 104, 17661-17674.

Whipple, K.X., Kirby, E. and Brocklehurst, S.H. (1999). Geomorphic limits to climate-induced increases in topographic relief. Nature, 401, 39-43.

Whitfield, R.G., Macklin, M.G., Brewer, P.A., Lang, A., Mau, B. and Whitfield (née Maher), E. (2013). The nature, timing and controls of the Quaternary development of the Rio Bergantes, Ebro basin, northeast Spain. Geomorphology, 196, 106-121.

Willet, S.D., Hovius, N., Brandon, M.T. and Fischer, D.M. (2006). Introduction. In Willet, S.D., Hovius, N., Brandon, M.T. and Fischer, D.M. (eds.). Tectonic, climate and landscape evolution. The Geological Society of America, 398, vii-xi.

Yang, G., Zhang, X., Tina, M., Brierley, G., Chen, A., Ping, Y., Ge, Z., Ni, Z. and Yang, Z. (2011). Alluvial terrace systems in Zhangjiajie of northwest Hunan, China: Implications for climate change, tectonic uplift and geomorphic evolution. Quaternary International, 233, 27-39.

Zaprowski, B.J., Pazzaglia, F.J. and Evenson, E.B. (2005). Climatic influences on profile concavity and river incision. Journal of Geophysical Research, 110, F03004, doi:10.1029/2004JF000138.

Zeyen, H. and Fernández, M. (1994). Integrated lithospheric modeling combining thermal, gravity, and local isostasy analysis: application to the NE Spanish Geotransect. Journal of Geophysical Research, 99, 18089-18102.

Figure captions

Figure 1. Location of the Cinca River drainage basin and the Ebro Basin in NE Iberia.

Figure 2. Geological setting of the Cinca River Valley in NE Iberia (A) and geological mapping of the bedrock (adapted from Barnolas et al., 2009) (B).

Figure 3. Distribution of terraces along the Cinca River valley (A). Detailed geomorphological maps and cross-sections of terraces in the Ainsa (B) and Albalate (C) sectors.

Figure 4. Field photographs of terraces in the Cinca River valley: alluvial cover of the terrace Qt7 overlaying Eocene marls near Ainsa (A) and Miocene clays and sandstones near Almudáfar (B); deposits of terrace Qt7 made of massive and cross-stratified gravels near Albalate (C); preserved staircase terrace sequences in the Ainsa (D), Monzón (E) and Binaced (F) sectors.

Figure 5. Grain size trends for Cinca River terrace deposits (Qt3, Qt7, Qt9) decreasing downstream.

Figure 6. Longitudinal profiles of the Cinca River terraces and the active channel. General parallel profiles with a subtle trend to divergence upstream are observed.

Figure 7. Paleomagnetic analysis. Natural remanent magnetisation of the Cinca Terraces (A), orthogonal demagnetisation diagrams of selected samples (B) and paleomagnetic means values in the studied terraces (C).

Figure 8. Fluvial incision rates in the Cinca River valley from successive preserved strath terraces at the upper reach (Ainsa sector) and at the lower reach (Albalate sector) of the valley. Spatial and temporal differences are clearly identified. Paleomagnetic timescale and marine isotope stages (adapted from Gibbard and Cohen, 2008) are included.

Table captions

Table 1. Terraces, numerical dates and heights at the Albalate and Ainsa sectors of the Cinca River valley.

Table 2. Summary of relative degrees of soil development on the Cinca River terrace surfaces and estimated ages.

Table 3. OSL dates from terraces in the the Cinca River valley (adapted from Lewis et al., 2009).

Table 4. Paleomagnetic data. Location and UTM coordinates (T30). n/N; considered/analysed samples. Pol: Polarity. Dec/inc: magnetic declination and inclination and the Fisher (1954) statistical parameters (a95 and K).

Table 5. Fluvial incision rates calculated from coupled preserved terraces in the Cinca River valley. Comparison of incision rates at the Ainsa and Albalate sectors is established. Temporal variations of incision rates at the Albalate sector are also evidenced.

Appendix captions

Appendix 1. Detailed geological map (including strath terraces) of the Cinca River valley. GPS measurements of elevation of terrace straths and active channel points are also indicated.

Appendix 2. Cinca River terrace strath data measurements and observations. UTM coordinates (latitude and longitude), elevation, substrate lithology (abbreviations: gyp, gypsum; ls, limestone; sst, sandstone), alluvium thickness (m), maximum grain size (Dmax), location and distance from headwaters are indicated. UTM coordinates and strath heights were obtained from a differentially corrected GPS accurate to 1 cm. Measurements from the headwaters of the river were obtained from topographic maps 1:25,000 in scale.

Fig. 1

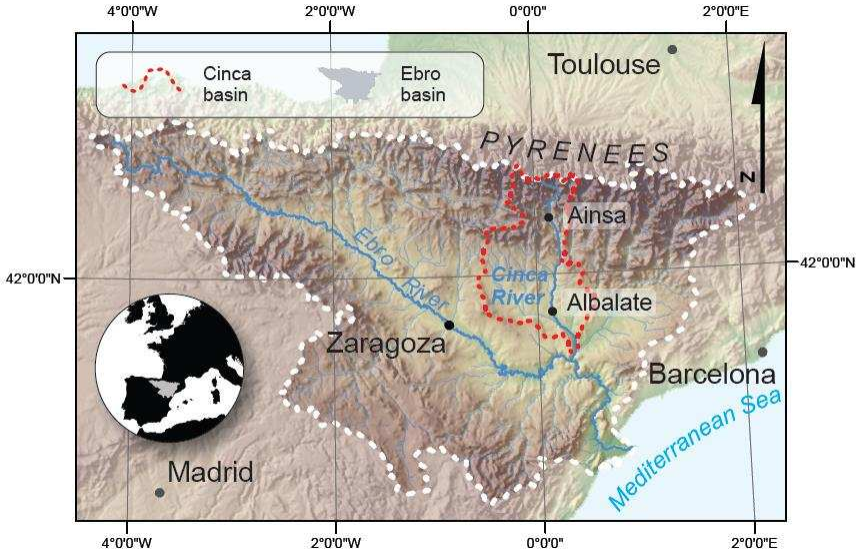

Fig. 2

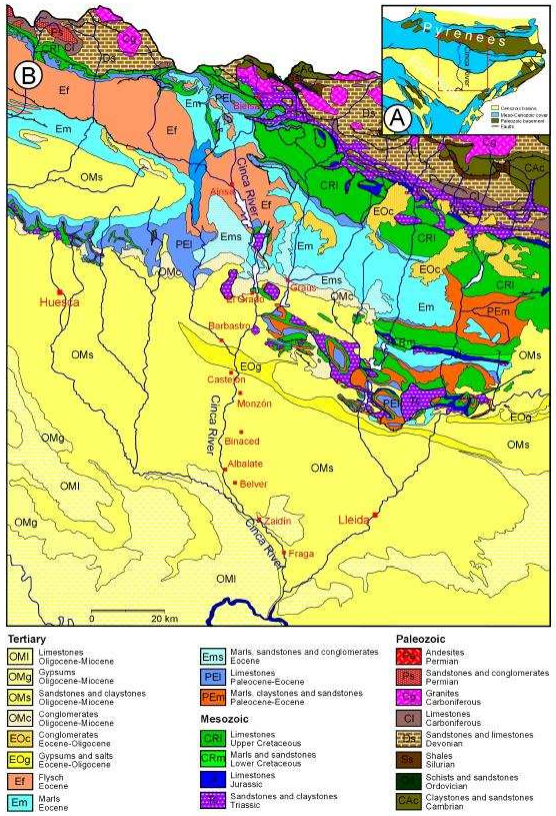

Fig. 3

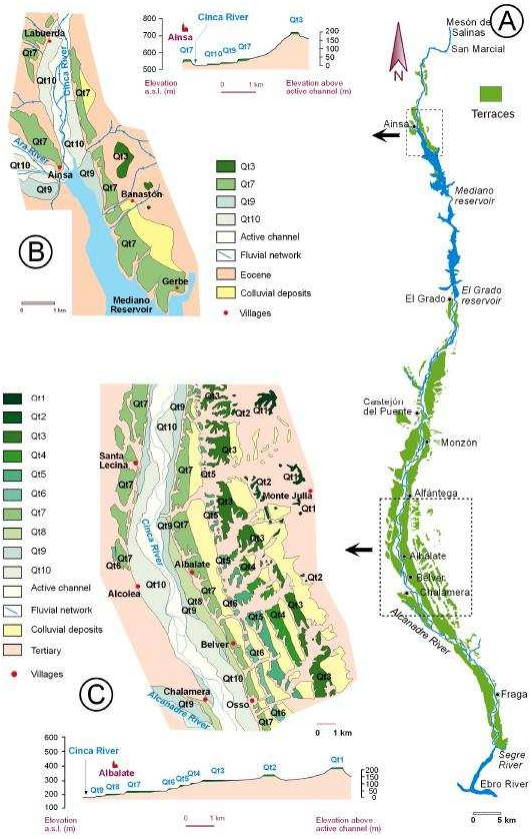

Fig. 4

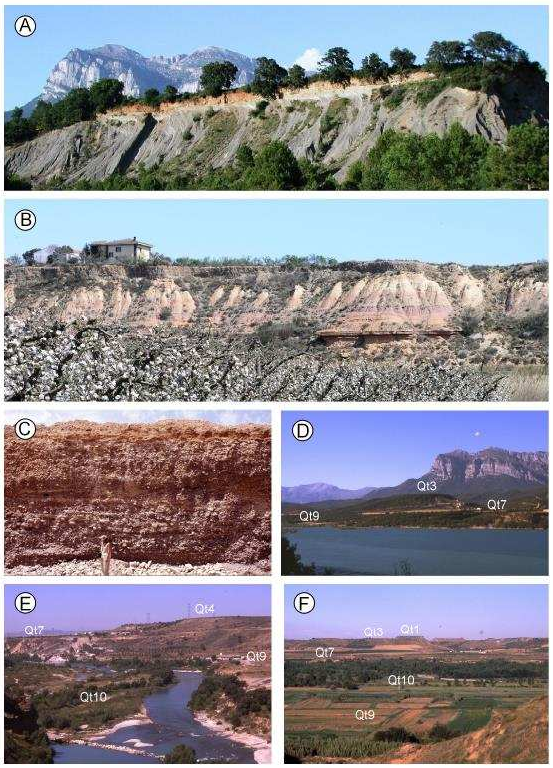

Fig. 5

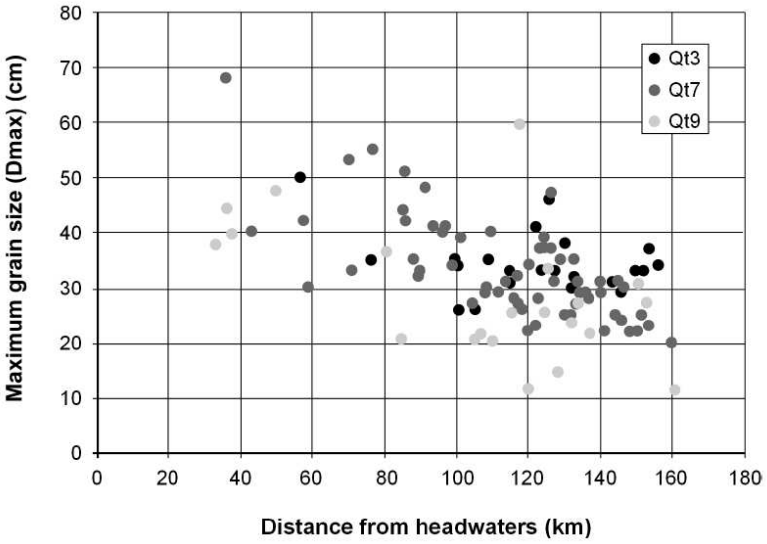

Fig. 6

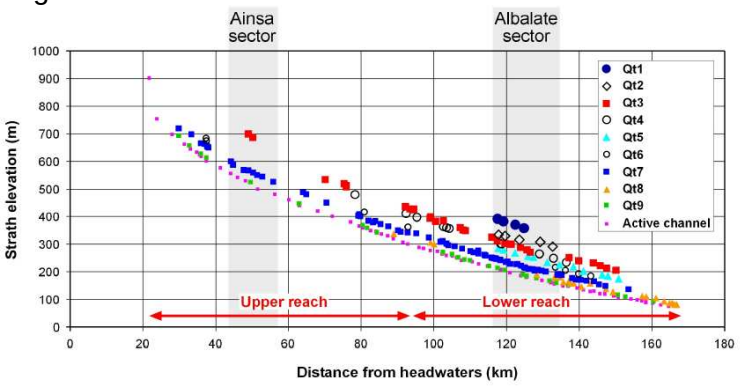

Fig. 7 below

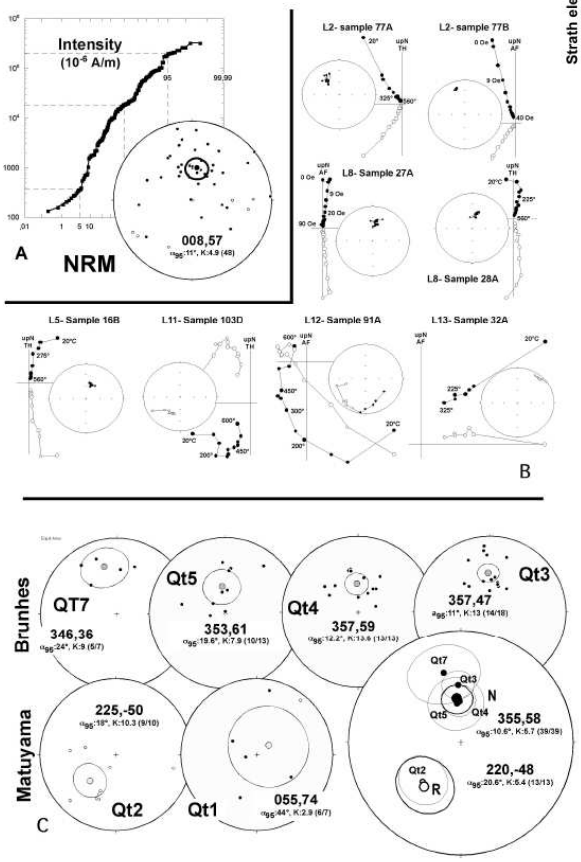

Fig. 8

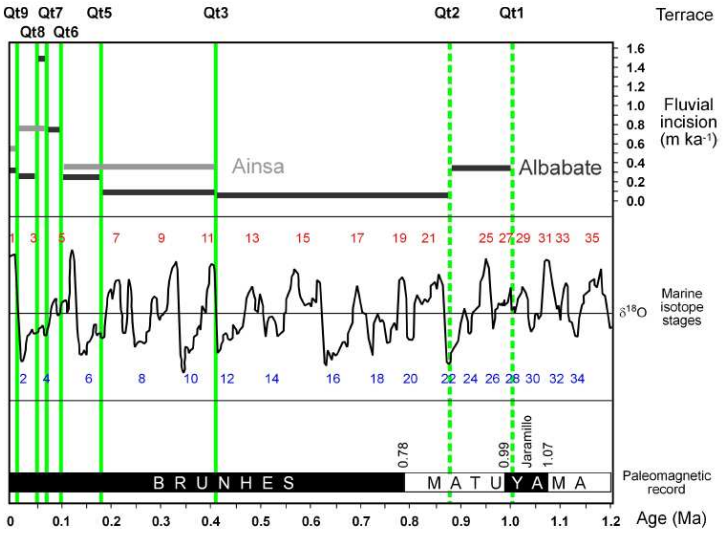

Appendix 1

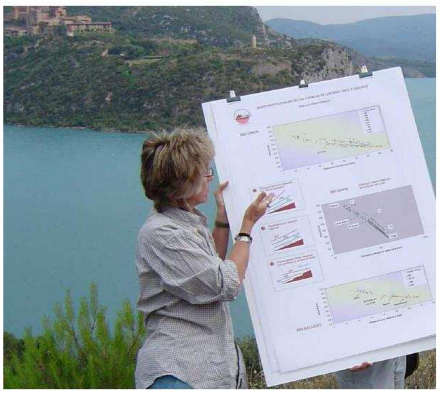

Table 1. Terraces, numerical dates and heights at the Albalate and Ainsa sectors of the Cinca River valley.

Terrace	Age (Ky)	Height (m)	
		Ainsa sector	Albalate sector
Qt1	999-1070[c]	-	182.1
Qt2	780-999[c]	-	132.5
Qt3	401±117[b]	172.5	103.5
Qt4	-	-	91.3
Qt5	178 ± 21[a]	-	79.9
Qt6	97±16[a]	-	60.4
Qt7	61 ± 4[a]	44.2	33.9
Qt8	47 ± 4[a]	-	13.1
Qt9	11 ± 1[a]	6.0	3.6

[a] Numerical age from Optical Stimulated Luminiscence (Lewis et al., 2009)
[b] Age derived from soil chronofunction used in Lewis et al. (2009)
[c] Tentative age from paleomagnetic data

Table 2. Summary of relative degrees of soil development on the Cinca River terrace surfaces and estimated ages.

Terrace	PDI Value Range (number of soils)[1]	Soil Age[2]	Source of Age[3]	MAX B Horizon Type[4]	MAX Carbonate Stage Morphology[5]
Albalate Sector					
Qt9	14.7-18.1 (2)	11±1	OSL	Bk-Bwk	I+
Qt8	23.2-24.7 (2)	47±4	OSL	Bk-Btk	I-II
Qt7	27.0-33.3 (5)	61±4	OSL	Btk-Bkm	II-III
Qt6	43.2 (1)	97±16	OSL	Btk	III+
Qt5	45.1-59.9 (3)	178±21	OSL	Bk-Bkm	III+-IV+
Qt3[6]	61.4-80.8 (5)	401±117	PDI	Bt-Bk-Bkm	IV-V+
Ainsa Sector					
Qt9	39.3 (1)	11±1	OSL	Btk	I
Qt7	64.4-67.9 (2)	61±4	OSL	Bt-Btk	I
Qt3	105.1 (1)	-	-	Bt	none

[1] Profile Development Index value and number of soils described shown in ( ). Minimum and maximum PDI values show when more than 2 soils
[2] Age of soil on terrace surface
[3] OSL: Optical Stimulated Luminescence, PDI: age derived from soil chronofunction used in Lewis et al (2009)
[4] Strongest, best develop B horizon type in each soil profiles. Subscripts shown are w: color or structure B; k: accumulation of carbonates; t: accumulation of clay; m: cemented
[5] Carbonate stage morphology from Gile et al. (1981) and Birkeland (1999)
[6] PDI values for the 5 Qt3 soils near Albalate are 61.4, 75.1, 64.9, 64.8, 80.8, respectively

Table 3. OSL dates from terraces in the Cinca River valley (adapted from Lewis et al., 2009).

Lab Code	Terrace	Northing	Easting	De (Gy)	Dose rate (mGy/a)	OSL date (ka)
X398	Qt5	4618380	266866	237±26	1.39±0.09	171± 22
X399	Qt5	4619473	266357	209±7	1.16±0.7	180±12
X397	Qt6	4618085	266253	157±23	1.62±0.11	97±16
X396	Qt7	4700762	265624	156±26	2.46±0.18	63±12
X1122	Qt7	4700762	265624	128±27	2.16±0.12	59±13
X823	Qt7	4678877	270913	82±15	1.28±0.08	64±13
X197	Qt7	4618846	265647	150±3	2.45±0.12	61±3
X199	Qt7	4613809	267775	101±5	1.80±0.09	56±4
X198	Qt7	4613809	267775	118±5	1.82±0.10	65±5
X817	Qt8	4624970	262087	89.0±10.2	2.26±0.14	39±5
X821	Qt8	4614698	267127	83±10	1.96±0.13	42±6
X833	Qt8	4598786	279236	117±6	2.50±0.16	47±4
X808	Qt8	4598765	278848	88±4	1.75±0.10	50±4
X809	Qt8	4598765	278848	90±2	1.79±0.11	50±3
X828	Qt9	270671	270671	18.3±1.1	1.86±0.12	10±1
X826	Qt9	266149	266149	21.8±0.7	1.89±0.13	12±1
X812	Qt9	266149	266149	18.0±7.6	1.46±0.07	9±4
X813	Qt9	266149	266149	27.0±3.6	1.91±0.10	14±2
X816	Qt9	261783	261783	26.5±1.8	2.15±0.14	12±1
X806	Qt9	263612	263612	23.0±2.3	2.03±0.11	11±1
X807	Qt9	263612	263612	22±1.4	1.96±0.10	11±1
X832	Qt9	275009	275009	18.4±3.6	1.81±0.12	10±2

Table 4
Paleomagnetic data. Location and UTM coordinates (T30). n/N; considered/analyzed samples. Pol: Polarity. Dec/inc: magnetic declination and inclination and the Fisher (1953) statistical parameters (a95 and K).

Terrace	Pit	X (30T)	Y (30T)	Locality	Samples	n	N	Dec	Inc	a95	K	Pol
Qt7	TA2-1	759,286	4,700,351	Ainsa (Polideportivo)	P85 to P90	3	3	329	32	26.7	33.6	N
	TA4-1	760,468	4,698,252	Banastón (Caballos)	P77 to P84	2	4	13	38	32.0	125.7	N
					PCA only	5	7	346	36	24.0	9.0	N
Qt5	T6-1	766,285	4,619,535	Belver (Plana Valentina)	P01 to P09	6	8	354	64	21.5	12.8	N
	T6-1	765,701	4,620,590	Belver (Granja Baillarin)	P10 to P15	4	5	350	56	54.3	5.1	N
					PCA only	10	13	353	61	19.6	7.9	N
Qt4	T7-1	766,023	4,622,346	Belver (Los Almendros)	P16 & P17	2	4	22	49	37.1	94.8	N
	T7-3	767,682	4,620,960	Belver (Silvio Ballarín)	P44 to P54	3	3	288	55	24.6	10.0	N
					PCA + demagnetization circles	13	13	357	59	12.2	13.6	N
Qt3	T8-1	764,028	4,628,305	Albalate (Los Olivos)	P18 to P24	4	4	26	25	49.7	5.9	N
	T8-2	763,799	4,627,424	Albalate (El Chopo)	blocks P25 to P28	10	11	5	51	12.0	18.9	N
	T8-4	764,028	4,628,305	Albalate (Las Lecineras)	P107 to P110	3	3	339	35	31.3	24.9	N
					PCA only	14	18	357	47	11.0	13.0	N
Qt2	T9-1	765,203	4,629,205	Albalate (Mombrun)	P55 to P57 + P68 to P70	3	3	153	− 71	87.3	4.6	R
	T9-2	765,126	4,628,812	Albalate (Mombrun)	P103 to P106	4	4	203	− 41	5.7	351.1	R
	T9-3	765,200	4,628,537	Albalate (Mombrun)	P91 to P102	3	3	275	− 37	22.9	11.4	R
					PCA + demagnetization circles	9	10	225	− 50	18.0	10.3	R
Qt1	T10-2	767,495	4,629,475	Albalate (San Salvador)	P29 to P34	6	7	55	74	44.0	2.9	N
	Cinca Terraces-Reverse					10	10	220	− 48	20.6	5.4	R
	Cinca Terraces-Normal					48	58	355	58	10.6	5.7	N
	Cinca Terraces-N + R					58	68	8	57	9.8	5.1	N + R

Table 5
Fluvial incision rates calculated from coupled preserved terraces in the Cinca River valley. Comparison of incision rates at the Ainsa and Albalate sectors is established. Temporal variations of incision rates at the Albalate sector are also evidenced.

Coupled terrace	Differential incision (m)	Elapsed time (Ka)			Incision rate (m/ky)		
		Mean	Minimum	Maximum	Mean	Minimum	Maximum
Qt3–Qt7 Ainsa	128.3	340	219	461	0.38	0.59	0.28
Qt3–Qt7 Albalate	69.6	340	219	461	0.20	0.32	0.15
Qt7–Qt9 Ainsa	38.2	50	45	55	0.76	0.85	0.69
Qt7–Qt9 Albalate	30.3	50	45	55	0.61	0.67	0.55
Qt9-Active channel Ainsa	6.0	11	10	12	0.54	0.6	0.5
Qt9-Active channel Albalate	3.6	11	10	12	0.33	0.36	0.3
Qt1–Qt2 Albalate	49.6	145[a]	no	no	0.34[a]	no	no
Qt2–Qt3 Albalate	29.0	488[a]	no	no	0.06[a]	no	no
Qt3–Qt5 Albalate	23.6	223	85	361	0.11	0.28	0.07
Qt5–Qt6 Albalate	19.5	81	66	108	0,24	0.29	0.18
Qt6–Qt7 Albalate	26.5	36	26	46	0.74	1.02	0.58
Qt7–Qt8 Albalate	20.8	14	22	6	1,48	0.94	3.45
Qt8–Qt9 Albalate	9.5	36	41	31	0.26	0.23	0.31
Qt9-Active channel Albalate	3.6	11	10	12	0.33	0.36	0.30

[a] Indicative data.

Y (m)	X (m)	Strath elevation (m)	Substrate	Max. rep. grain size (cm)	Location	Distance from headwaters (km)
Qt1 strath						
4626238,7	268814,2	357,31	sst, clay	48	Monte Julia	130,40
4628762,5	268160,6	369,94	clay, sst	48	San Salvador	128,00
4631710,0	266994,0	382,77	clay, sst	43	Brujas	124,70
4633561,1	266598,0	391,65	clay, sst	30	Binaced, pine	123,10
				mean = 42 ± 9		
Qt2 strath						
4622779,0	269090,4	291,86	clay	40	Belver	138,20
4626128,2	267180,0	307,69	sst	42		134,80
4627915,5	266335,7	316,46	clay, sst	48	Mombrun	129,05
4631605,1	265448,4	329,24	clay	36	Binaced 2	125,15
4633506,8	265338,9	333,99	clay, sst	39	Binaced 1	123,35
				mean = 41 ± 4		
Qt3 strath						
4606834,7	275456,5	204,54	clay	34	Zaidin south	155,65
4609076,4	274022,9	212,25	clay	37	Zaidin	153,10
4610459,5	272542,3	221,32	clay	33	San Anton	151,30
4612664,1	272105,5	231,46	ls, clay	33	Zaidin north, peaches	149,45
4615680,8	270893,7	239,25	clay	29	Almudafar	145,45
4617633,2	269497,0	251,03	clay	31	Osso	142,79
4624783,7	265615,0	269,81	clay	32	Albalate, Porquet	132,10
4625718,6	264849,8	278,70	sst	30	Lecineras south	131,25
4627553,2	264705,4	287,57	clay, sst	38	Lecineras north	129,45
4629600,5	264481,2	299,33	clay	33	Las Brujas west	126,85
4630292,1	264604,0	300,16	clay	33	Las Brujas west	126,60
4631856,3	263793,9	302,45	clay	46	Alfantega-Albalate	125,15
4633829,1	264075,3	312,84	sl, sst	33	Alfantega south	123,05
4635456,3	264683,0	324,76	sst, clay	41	Alfantega north	121,60
4641433,4	267164,4	348,76	sst	33	Monzon south	114,30
4642139,0	267230,3	351,28	clay	31	Monzon, cemetary	113,60
4643345,2	267354,5	359,67	clay	NA	Monzon, castle	112,80
4648994,7	264935,1	384,64	sst clay	35	Castejon, gravel pit	108,20
4650942,7	264077,2	382,30	gyp	NA	Castejon-Salinas	106,10
4651648,2	264273,7	398,07	gyp	NA	Castejon	104,70
4652887,4	269341,9	393,82	clay	26	Fonz 3	104,55

4656953,7	265155,5	427,86	sst, clay	26	Las Coronas 3	100,05
4657059,2	265420,3	424,30	clay, sst	34	Las Coronas 1	99,95
4657890,1	265794,1	427,42	clay, sst	35	Las Coronas 4	98,95
4659224,5	266451,3	435,14	cgl, sst	NA	Las Coronas 2	97,80
4673397,6	270716,4	507,73	cgl	NA	Torreciudad 2	81,55
4673470,8	270762,6	511,44	cgl, clay	NA	Torreciudad	81,55
4674106,1	270586,2	519,12	clay	NA	Torreciudad north	80,90
4679386,0	270652,0	533,57	clay	35	Abizanda-Moscarazos	75,70
4698766,8	267451,0	687,52	sst, marls	50	Santa Tecla	55,80
4698820,7	267324,8	685,63	marls	NA	Santa Tecla	55,80
4699527,8	267293,3	698,75	marls, sst	NA	Arnal	54,55
				mean = 34 ± 6		
Qt4 strath						
4618310,2	268999,2	234,51	clay	41	Osso	142,00
4621360,8	267202,7	249,02	clay	27	Belver	138,50
4623856,0	265718,1	264,08	clay	31	Albalate	134,65
4632761,8	263831,0	299,94	clay, sst	41	Alfaltega south	124,20
4633014,6	263912,7	301,32	cl	43	Binaced road	123,95
4647516,3	264286,8	356,10	clay, sst	26	Castejon, horse arena	109,85
4648272,3	264594,9	360,26	sst, clay, gyp	NA	Castejon 1	109,05
4648923,5	265099,9	363,73	sst	NA	Castejon, gravel pit	108,20
4654312,1	269983,2	397,45	clay	NA	Fonz 1	100,95
4657383,2	270205,3	410,16	clays	NA	Fonz 2	97,95
4671239,3	271297,4	478,68	cgl, sst, clays	NA	El Grado	83,90
				mean = 35 ± 8		
Qt5 strath						
4604667,1	276619,5	175,11	clay, sst, lm	28	Pilaret-Fraga 1	158,35
4606841,1	275133,3	185,07	clay, marls	36	Zaidin south	155,45
4608012,4	273923,2	189,64	clay	NA	Zaidin	153,85
4612314,6	270700,4	202,56	clay, sst	39	Zaidin	148,70
4615106,6	269791,6	219,61	clay	51	Almudafar	146,00
4617641,2	268022,3	226,21	clay	29	Osso	142,10
4620596,2	266439,1	235,60	clay	38	Belver	138,70
4623348,5	264910,9	254,56	clay, sst	46	Albalate	134,90
4625398,1	264561,8	257,27	clay	NA	Lecineras	131,50
4627116,2	264081,3	268,53	clay	37	Clamor	129,90
4629659,3	263752,5	279,92	clay	37	Alfantega-Albalate 2	126,75
4631764,0	263530,5	285,61	sst, clay	41	Alfantega-Albalate 1	125,30
				mean = 38 ± 7		

Qt6 strath

4612095,2	270574,9	184,55	clay	31	Zaidin	148,80
4614561,5	268279,5	192,57	clay	24	Almudafar	145,40
4617395,8	266899,7	205,17	clay	38	Osso	141,75
4619988,9	265939,2	215,59	clay, sst	46	Belver	139,00
4662716,8	271705,9	362,57	sst, marls	30	Estada	98,45
4668560,4	272171,0	416,16	sst	27	Artasona	86,45
4710107,9	264958,2	673,64	not seen	80	Laspuna	43,05
4710475,2	265867,2	683,96	marls	NA	Laspuna	42,90
				mean = 39 ± 19		

Qt7 strath

4603962,4	276944,5	136,17	clay, silt	20	Pilaret	159,15
4608542,3	272710,3	148,99	ls	23	Zaidin south	152,80
4609939,6	271780,7	154,18	ls, clays	25	Zaidin	151,00
4611129,6	270605,8	165,74	clay, ls	22	Ave	149,60
4612328,1	269279,9	167,12	clay	22	Almudafar south	147,55
4613510,6	268000,6	171,28	clay	30	Almudafar south 2	145,95
4613818,8	267774,6	170,83	sst?	24	Almudafar, gravel pit	145,55
4614506,9	267304,1	172,25	sst, clay	31	Almudafar north	144,65
4615711,5	266825,8	177,04	ls, clay	25	Osso south	143,60
4617975,1	266027,5	188,40	cl?	22	Osso north	140,75
4618821,2	265551,1	190,81	sst, ls, clay	29	Belver, Tejerias	139,75
4619145,8	265392,6	189,07	clay	31	Belver	139,65
4621596,7	264063,9	199,87	sst, silt	28	Albalate	136,35
4621619,2	264052,5	199,71	sst, silt	NA	Albalate	136,35
4622728,3	263753,3	204,00	silt, sst	29	Albalate	135,20
4623531,0	263013,5	207,42	clay, sst	29	Albalate	134,20
4623528,9	259973,4	203,89	silt, clay	31	Alcolea	133,25
4625094,6	259311,4	209,43	clay	27	Alcolea north	132,74
4624817,7	262567,7	208,95	clay	35	Albalate km 1	132,30
4625514,2	259383,6	209,85	clay	NA	Alcolea north 2	131,65
4626568,0	259527,9	213,21	clay?	25	Santa Lecina, Viruelas	130,70
4626521,5	262161,2	216,06	clay, sst	25	Albalate km 3	130,45
4629220,0	260490,3	222,01	sst	25	Santa Lecina south	129,60
4628634,8	262493,1	228,18	sst, clay	NA	Albalate km 5.5	128,60
4628801,0	262431,0	226,97	clay	NA	Albalate km 6	128,30
4628801,1	262430,8	227,67	clay	35	Albalate km 6	128,30
4630222,5	260538,4	228,20	clay	31	Santa Lecina north	126,60
4631295,0	262957,6	235,87	sst, clay	47	Albalate km 8	125,85

4631388,9	263081,3	237,28	sst	37	Albalate km 8	125,85
4631924,0	260920,1	234,55	st, clay	NA	Estiche south	125,45
4633048,6	263181,9	241,37	clays	37	Binaced road	123,95
4633660,7	260901,2	242,52	clay, sst	39	Estiche	123,80
4634429,6	263302,9	246,29	clay	37	Alfantega south	122,77
4635076,2	263518,3	248,91	clay	28	Alfantega	122,45
4635076,0	263519,1	248,84	clay	NA	Alfantega	122,05
4635999,8	261450,7	250,32	clay, sst	23	Estiche north	121,50
4637344,9	263780,0	258,93	sst, clay	34	Pueyo	119,85
4637984,2	261620,5	261,21	clay	22	Pomar north	119,50
4639441,3	264658,1	269,06	sst, clay	NA	Pueyo	117,80
4639697,2	262563,3	265,73	clay, sst	NA	Conchel south 2	117,80
4639713,5	262565,1	276,29	clay, sst	26	Conchel south 2	117,80
4640762,0	263112,8	269,41	sst, clay	27	Conchel	116,65
4640326,8	264903,1	270,19	clay, sst	32	Alegria	116,55
4641521,3	263719,4	274,05	sst	28	Conchel north	115,65
4643649,4	264741,5	283,85	sst	31	Selgua	113,35
4645806,7	265061,4	292,63	clay, sst	29	Monzon north	111,25
4647577,6	265271,7	295,37	sst, clay	NA	Castejon, concrete plant	109,55
4647937,3	265274,5	302,00	sst	NA	Castejon (repeat)	109,05
4647937,5	265275,1	302,98	sst, clay	40	Castejon	109,05
4648783,4	266670,7	310,82	not seen	NA	Chula Vista	107,95
4648737,8	266624,3	309,66	sst, clay	NA	Chula Vista	107,95
4648783,4	266670,7	310,82	sst, clay	30	Chula Vista	107,95
4649518,1	267381,8	307,92	gyp	29	Ariestolas	107,45
4653028,9	268364,0	324,47	clay?	27	Cofita	104,15
4655141,4	267896,4	338,23	sst	39	Fonz	100,80
4657703,6	267937,3	341,73	sst, cgl, clay	34	Arias II	98,40
4658881,1	268853,8	344,51	cgl	41	Casa Pararayos	96,50
4659779,8	269184,5	349,60	sst	40	Central Electrica Pilas	95,70
4662686,0	269983,7	364,44	clay, sst	41	Enate	93,10
4664323,9	270860,5	372,14	clay, sst	48	Enate north	90,90
4665668,4	271111,9	383,23	cgl, sst	33	El Grado south	89,45
4666272,9	271795,1	378,93	sst, cgl	32	Olvena	88,90
4667415,4	271756,1	385,12	sst, cgl	35	Artasona south	87,60
4669740,5	270777,3	400,65	clay	42	El Grado	85,35
4670069,9	271665,4	408,35	sst	51	El Grado dam 2	85,05
4670299,3	271420,3	402,16	ls	44	Dam	84,75
4678793,0	270908,2	449,57	marls?	55	Moscarazos	76,05
4684220,2	270139,2	479,93	ls, marls	33	Liguerre	70,50

4685135,5	270156,0	488,43	Triassic red beds	53	Liguerre2	69,60
4692888,6	268198,3	525,39	marls	NA	Ainsa, airport	61,40
4696062,9	267620,1	543,96	marls	30	Gerbe	58,45
4697188,3	266541,9	550,44	sst, marls	42	Banaston	57,00
4698268,3	266398,0	559,25	marls	NA	Banaston 2	55,85
4699552,2	266071,0	566,39	sst	NA	Usana	54,55
4700761,5	265623,9	568,12	marls	NA	Pueyo-Ainsa	53,30
4703367,9	265076,6	587,06	marls	NA	Ainsa north	50,40
4703968,8	264325,4	599,71	marls	NA	Labuerda	49,80
4709582,2	265366,6	650,20	marls	NA	Escalona	43,60
4709906,5	265387,2	653,19	marls	NA	Escalona2	43,25
4709912,6	265032,2	655,82	marls	NA	Escuain hwy	43,20
4710744,3	265700,3	662,57	marls	40	Laspuna	42,55
4711889,9	265799,1	664,36	marls	NA	Laspuna north	41,45
4714062,0	266742,2	697,85	ls	NA	Misuellas	38,90
4713888,6	269696,5	718,61	marls	68	Badiain	35,40
				33 ±9		
Qt8 strath						
4590370,1	279052,3	80,17	ls	NA	Escarpe, convent	172,40
4590370,5	279052,6	80,24	ls	NA	Escarpe, convent	172,40
4590891,4	279123,9	80,10	ls	25	Masalcorreig	171,80
4590945,9	279117,4	81,53	ls	NA	Masalcorreig	171,80
4591745,5	279254,7	86,95	ls	NA	Masalcorreig	171,05
4592329,1	279302,0	85,93	marls, ls	23	Masalcorreig south	170,35
4593975,4	279633,5	91,86	sst, clay	27	Masalcorreig north	168,85
4597707,6	279414,7	105,00	clay,sst	NA	Fraga south	166,65
4598786,9	279212,5	108,89	clay,sst	NA	Fraga hwy work	163,95
4599957,9	278910,1	111,15	sst, clay	NA	Fraga	162,90
4606658,0	274037,9	125,52	clay, sst, ls	NA	Clamor, confluence	154,85
4607369,5	271680,2	137,35	clay	28	Velilla	152,90
4610224,5	268472,5	158,00	clay	25	Velilla, Ave	148,55
4612890,9	267490,8	145,63	clay	31	Almudafar south	146,15
4615161,1	266942,4	158,30	clay, sst	25	Almudafar north	144,05
4614753,1	265034,6	157,11	clay, marls	25	Chalamera-Ballobar	143,10
4616088,7	266511,0	166,68	clay	NA	Osso	142,65
4617565,5	265856,2	162,10	clay	35	Osso north	141,15
4617332,9	263643,4	180,52	clay	42	Chalamera	140,15
4618685,0	262929,1	179,86	clay	36	Chalamera, hermitage	138,75
4624667,5	262009,9	188,57	?	22	Albalate	133,90
4651338,4	267816,2	299,06	gyp	28	Cofita south	105,65

4652421,1	267841,3	305,88	gyp, marls	27	Cofita, canal	104,65
4660668,2	269984,0	336,43	Keuper facies	NA	Estadilla	94,50
				mean = 29 ± 6		
Qt9 strath						
4596667,0	279164,7	93,79	clay, sst	12	Fraga toll rd	160,45
4603299,3	275311,1	101,25	sst, clay	28	Miralsot south	152,75
4605605,7	275012,0	116,38	sst, clay	31	Zaidin south, gravel pit	150,60
4615652,4	265127,9	152,28	clay?	22	Chalamera-Ballobar	136,95
4618197,2	263357,3	159,90	sst, clay	28	Chalamera, hermitage	133,70
4620341,8	264057,6	168,05	clay	24	Albalate-Belver	131,85
4623545,6	262027,5	177,68	?	15	Albalate	128,25
4626222,8	261433,0	184,79	sst	34	Las Torres	125,50
4627246,1	261894,9	190,18	sst	26	Ciguena	124,50
4632191,0	262278,6	205,64	sst	12	Soto del Tros north	119,40
4633967,1	262899,7	213,73	clay, sst	60	Alfantega	117,55
4636516,8	262991,4	220,84	cl	26	Pueyo	115,25
4641308,4	264711,2	241,67	sst	21	Alegria	110,00
4642910,2	265578,5	244,41	sst	NA	Monzon south	108,40
4644355,7	266152,6	251,55	sst, clay	22	Sosa confluence	106,70
4646366,6	265770,4	263,05	sst	21	Monzon north	105,05
4648800,4	266119,5	267,70	sst	NA	Castejon 2	102,45
4648906,0	266183,6	271,11	sst	NA	Castejon 1	102,45
4665046,2	272113,9	341,86	not seen	21	Esera confluence	84,35
4667582,6	270679,9	358,33	not seen	NA	El Grado south	81,70
4669267,9	270600,1	369,16	not seen	37	El Grado south	80,40
4686475,7	270644,5	446,97	ls	NA	Liguerre, bridge	62,95
4698725,7	265976,7	524,26	marls (approx.)	48	Usana	49,60
4710107,5	265784,0	612,75	marls	40	Laspuna	37,50
4711924,7	265460,0	627,23	marls	45	Laspuna	35,90
4714416,3	266839,4	657,03	marls	38	Hospital de Tella	32,75
4714170,9	269863,3	692,99	ls, marls	NA	Lafortunada	29,90
				mean = 29 ± 12		
Active channel						167,50
4590568,2	278243,3	76,16		NA	Torrente south	166,50
4592675,2	279204,4	74,58		NA	Masalcorreig	164,60
4594870,8	278388,8	79,66		NA	Torrente de Cinca	162,50
4596928,2	278849,5	86,71		NA	Fraga toll rd	160,20
4598806,7	278948,2	91,45		NA	Fraga	158,35

4598821,9	278940,5	87,89		NA	Fraga circunvalacion	158,35
4600248,2	278725,2	94,51		NA	Fraga	157,25
4601693,1	278159,6	98,36		NA	Zaidin-Fraga 4	155,95
4603247,8	277358,1	101,14		NA	Zaidin-Fraga 3	154,25
4604209,4	276322,3	106,41		NA	Miralsot south	152,70
4605611,4	274968,5	105,92		NA	Zaidin south, gravel pit 2	150,75
4606472,3	274068,0	112,86	ls	NA	Zaidin-Fraga 2	149,55
4608479,0	272650,7	119,77		NA	Zaidin 1	147,05
4609465,8	271366,8	120,59	ls	NA	Zaidin	145,70
4610187,2	269704,0	129,27		NA	Ave south	144,05
4610378,3	268514,1	128,03		NA	Ballobar, Ave	143,00
4612062,3	267550,6	133,60		NA	Almudafar south	141,15
4613488,6	266644,3	140,72		NA	Almudafar	139,45
4615639,9	265193,2	147,30		NA	Chalamera-Ballobar	137,00
4616710,9	264612,4	148,82		NA	Chalamera	135,55
4618298,0	263415,2	155,20		NA	Chalamera, hermitage	133,20
4618566,0	263392,3	160,45		NA	Belver	133,40
4619667,1	263075,0	166,23		NA	Belver north	132,30
4620039,9	262992,4	159,69		NA	Albalate south	132,22
4622262,0	262463,6	169,12		NA	Albalate south	129,75
4623423,1	261865,3	176,13		NA	Albalate	128,30
4623430,2	261865,1	175,24		NA	Albalate	128,35
4626195,7	261399,3	180,14	sst	NA	Las Torres	125,50
4627618,6	261822,7	185,31	sst	NA	Ciguena	123,95
4630745,8	261361,0	196,13		NA	Soto del Tros	120,95
4633356,8	261767,0	207,86		NA	Estiche	118,35
4637273,7	262133,7	221,03		NA	Pomar	114,80
4639503,1	262665,8	228,24		NA	Pueyo	112,35
4640927,9	263980,0	235,68		NA	Conchel	110,60
4643437,3	265673,5	241,04		NA	Selgua-Monzon	107,60
4644809,6	265867,9	250,61		NA	Monzon	106,35
4646194,6	265594,6	257,47		NA	Monzon north	105,15
4648060,5	265631,7	258,81		NA	Castejon	103,40
4648969,3	266539,5	263,55		NA	Castejon 2	102,20
4650585,0	265670,5	273,82		NA	Castejon 3	101,05
4652004,2	265839,1	277,07		NA	Cofita	99,10
4653915,1	265547,3	285,08		NA	Vero confluence	97,20
4655130,7	266128,3	288,41		NA	Vero confluence north	96,00
4658190,6	266885,9	299,79	sst, cgl dipping 45N	NA	Arias ll	92,85
4659504,4	267534,9	306,99		NA	Coronas north	91,50

4660935,1	269750,3	319,45	NA	Puente las Pilas	88,90
4662402,9	270235,1	329,67	NA	Enate 2	87,35
4663979,8	271147,6	336,60	NA	Enate	85,60
4665299,6	271386,7	346,06	NA	Piscifactoria	84,10
4666952,5	271084,7	349,10	NA	Artasona south	82,65
4669068,8	271402,9	358,94	NA	El Grado	80,50
4670028,2	271513,5	365,31	NA	El Grado dam	79,50
4672400,0	271300,0	380	NA		77,15
4677400,0	271000,0	400	NA		72,10
4681300,0	272500,0	420	NA		68,10
4686300,0	274000,0	440	NA		63,05
4889100,0	270000,0	460	NA		60,15
4692750,0	268750,0	480	NA		56,30
4696800,0	266450,0	500	NA		51,55
4699976,5	264920,2	528,59	NA	Ainsa	48,25
4702081,1	264805,0	541,17	NA	Ainsa north	46,05
4704007,1	264807,9	555,85	NA	Labuerda	44,15
4706553,1	265675,7	575,91	NA	Labuerda north	41,35
4710050,0	265753,7	601,17	NA	Laspuna, bridge	37,50
4711829,8	265405,3	617,64	NA	Laspuna north	36,00
4711989,0	265561,9	623,30	NA	Puertolas	35,60
4712750,6	266107,4	633,25	NA	Puertolas north	34,80
4713987,4	266833,0	644,17	NA	Misuellas	33,15
4714366,8	268440,4	661,44	NA	Laspuna reservoir	31,40
4715470,8	270601,9	697,83	NA	Devotas	28,05
		740	NA		25,70
4718416,4	270829,7	753,47	NA	Salinas	25,05
		780	NA		23,70
		800	NA		23,45
4720183,9	273539,0	900,84	NA	Bielsa south, gorge	21,70
4723000,2	272895,7	973,66	NA	Bielsa	18,65
4724306,0	271381,9	1087,65	NA	Javierre	16,45
4725075,8	268267,4	1161,20	NA	Pineta 2	12,95
4729158,6	261407,7	1273,24	NA	Pineta	5,25
		1300	NA		4,25
		1400	NA		3,75
		1500	NA		3,35
		1600	NA		2,95
		1700	NA		2,75
		2100	NA		2,25

2200	NA	2,10
2500	NA	1,25
2520	NA	0,75
2600	NA	0,25
2700	NA	0,03